Jointly Active and Passive Beamforming Designs for IRS-Empowered WPCN

Zheng Chu, *Member, IEEE*, Pei Xiao, *Senior Member, IEEE*, De Mi, *Senior Member, IEEE*, Cheng Yin, *Member, IEEE*, Wanming Hao, *Senior Member, IEEE*, Wei Liu, *Senior Member, IEEE*, and Arismar Cerqueira Sodre Jr.

***Abstract*—This paper studies an intelligent reflecting surface (IRS)-empowered wireless powered communication network (WPCN) in Internet of Things (IoT) networks. In particular, a power station (PS) with multiple antennas uses energy beamforming to enable wireless charging to multiple IoT devices, in the downlink wireless energy transfer (WET) phase; then, during the uplink wireless information transfer (WIT) phase, these IoT devices utilise the harvested energy to concurrently transmit their individual information signal to a multi-antenna access point (AP), which equips with multi-user decomposition (MUD) techniques to reconstruct the IoT devices' signal. An IRS is deployed to improve the energy collection and information transmission capabilities in the WET and WIT phases, respectively. To examine the performance of the system under study, We maximize the sum throughput with the aim of jointly designing the optimal solutions for the active PS energy beamforming , AP receive beamforming, passive IRS beamforming, and time scheduling. Due to the multiple coupled variables, the resulting formulation is non-convex, and a two-level scheme to solve the problem is proposed. At the outer level, a one-dimensional (1-D) search method is applied to find the optimal time scheduling, while at the inner level, an iterative block coordinate descent (BCD) algorithm is proposed to design the optimal receive beamforming, energy beamforming, and IRS phase shifts. In particular, the receive beamforming part is designed by considering the equivalence between sum rate maximisation and sum mean square error (MSE) minimisation, thereby deriving a closed-form solution. Furthermore, we alternately optimize the energy beamforming and IRS phase shifts using Lagrange dual transformation (LDT), quadratic transformation (QT), and alternating direction method of multipliers (ADMM) methods. Finally, numerical results are presented to showcase the performance of the proposed solution and highlight its advantages compared to some typical benchmark schemes.**

***Index Terms*—Intelligent reflecting surface (IRS), wireless powered communication networks (WPCNs), mean square error (MSE), Lagrange dual transformation (LDT), quadratic transformation (QT), and alternating direction method of multipliers (ADMM)**

Z. Chu was with Institute for Communication Systems (ICS), Home for 5GIC & 6GIC, University of Surrey, Guildford, Surrey, GU2 7XH, United Kingdom, and is now with the Department of Electrical and Electronic Engineering, University of Nottingham Ningbo China, Ningbo 315100, China. (Email: andrew.chuzheng7@gmail.com)

P. Xiao and C. Yin are with Institute for Communication Systems (ICS), Home for 5GIC & 6GIC, University of Surrey, Guildford, Surrey, GU2 7XH, United Kingdom. (Email: p.xiao@surrey.ac.uk, c.yin@surrey.ac.uk)

D. Mi is with the College of Computing, Birmingham City University, Birmingham B4 7XG, United Kingdom. (Email: de.mi@bcu.ac.uk)

W. Hao is with the School of Electrical and Information Engineering, Zhengzhou University, Zhengzhou 450001, China, and also with the SongShan Laboratory, Zhengzhou 450018, China. (Email: iewmhao@zzu.edu.cn)

W. Liu is with the School of Electronic Engineering and Computer Science, Queen Mary University of London, Mile End Road, London E1 4NS, United Kingdom. (Email: w.liu@sheffield.ac.uk).

Arismar Cerqueira Sodr, Jr., are with the Laboratory WOCA (Inatel), Santa Rita do Sapuca 37540-000, Brazil (Email: arismar@inatel.br).

I. Introduction

Advanced information and communications technologies (ICT) empower the next-generation Internet of Things (IoT) networks, enabling various types of smart device (SD) connectivities with higher spectral and energy efficiencies, and supporting diverse vertical industries, e.g., smart factory/home/healthcare, mission-critical public-safety networks, and intelligent transportation [1]. An IoT network consists of an access point (AP) and multiple SDs, and the AP collects, analyzes and processes the data from these devices over the Internet. While these SDs are rapidly proliferating in the real world, existing IoT networks refuse to support massive wireless connectivity when they rely on the traditional multiple access (MA) techniques. The main challenge restricting the wireless connectivity lies in two aspects, i.e., energy constraint and information constraint [1].

In most IoT applications, SDs have low energy capacity, traditionally charged by power sources/batteries with limited energy capacity, and require regular upkeep to maintain their lifespan. The cost of this maintenance is considerably high and sometimes even impossible for the SDs deployed in harsh environments [2]. On the other hand, current research efforts are mainly focused on energy-efficiency requirements, while the issue of energy constraints of the SDs continues to be a challenge in IoT networks. Given the advances of radio frequency (RF) energy harvesting, the concept of named wireless powered communication networks (WPCN) is considered as one of the potential energy-efficient solutions for SDs in IoT networks [3], [4]. In WPCN, SDs can be powered wirelessly from a stable power source, i.e., power station (PS), during the phase of downlink wireless energy transfer (WET), and then use the collected energy to deliver information to an AP during the phase of uplink wireless information transfer (WIT) [5]. Due to this transmission structure, the PS in the WPCN can be regarded as an alternative to the traditional battery equivalent, which not only effectively increases the energy efficiency of SDs, but also circumvents expensive maintenance and periodic replacement costs.

In addition to the energy constraint, information constraints represent another challenging task for low-power SDs. This mainly stems from two aspects: the need for more data and the controllable wireless propagations, both of which aim to guarantee a sufficiently high data rate for future IoT networks. Current techniques, e.g., millimeter-wave (MmWave)

and massive multiple-input multiple-output (massive MIMO), operate mainly in the high frequency bands and rely on a large number of RF chains at the AP, respectively, to achieve high data rate/spectral efficiency [6], [7]. This however incurs more energy consumption and higher hardware complexity. In conventional wireless networks, propagation channels are typically treated as a random and uncontrolled medium, which requires optimal transceiver strategies, i.e., beamforming designs, and power control algorithms [7]. Although these transceiver strategies can overcome the signal attenuation induced by fading channels, the channels are not yet reconfigurable, which should be fully exploited in future IoT networks. To iron out these two issues, a novel concept has been proposed, namely *intelligent reflecting surface* (IRS). The IRS is composed of a large number of passive reflecting elements/units to match the channel phase of a cascaded link of AP-IRS-SDs to the phase of the direct link of AP-SDs by dynamically controlling its reflection coefficients [8]–[10]. Due to their passive nature, the IRS-assisted wireless networks are proven to improve energy efficiency and achievable rate/throughput compared to conventional networks. The IRS operates in full-duplex (FD) mode and can simultaneously receive and reflect the energy/information signal.

A. The State-of-Art

The current research endeavours exploit the synergy between IRS and wireless powered IoT (WP-IoT) networks in a variety of contexts [11]–[23]. The overview in [11] aimed to present the performance gains of IRS in spectral efficiency without sacrificing energy efficiency. In [12]–[14], the IRS-assisted WPCN was investigated, where the energy harvesting capability of IoT devices was enhanced by the IRS passively participating in the downlink WET. In the uplink WIT, with the aid of IRS, these devices utilised the collected energy for information delivery in the manners of time-division multiple access (TDMA) [12], frequency-division multiple access (FDMA) [13], or non-orthogonal multiple access (NOMA) [14]. In addition, two novel transmission schemes, e.g., time switching and power splitting, were investigated in [15], [16]. Specifically, the circuit operation of IRS controller was supported by the RF harvested energy radiated by the PS, allowing the downlink WET to be divided into two portions for energy harvesting at the IRS and IoT devices. The work in [17] aimed to maximise the system throughput of an IRS-assisted WP-NOMA network with a co-located hybrid AP (H-AP). The downlink and uplink IRS passive beam patterns are attained based on an alternating optimisation (AO) approach, confirming that both IRS beam patterns are identical to achieve its optimality. A similar multi-group scenario was reported in [18], which separated all IoT devices into different groups. For the uplink WIT, these groups employ the TDMA protocol, while all IoT devices in a group share one sub-time duration to use the NOMA protocol. Three IRS beam patterns, i.e., full dynamic, partial dynamic, and static IRS beamformers, were considered for the downlink WET and uplink WIT [19], where a power splitting structure was considered in multiple rectifiers of the NLEH model to avoid input RF power in the saturated region; the transmit energy at the H-AP was minimised to jointly design the time scheduling, H-AP's transmit power, power splitting factor, and IRS passive beam patterns. In [20], the authors evaluated the impact of IRS phase shift error (PSE) and transceiver hardware impairment (THI) on system throughput of the IRS-assisted WPCN. By jointly optimising the PSE, IRS passive beam patterns, and time allocations, significant benefits can be gained by adjusting he phase shifts of the IRS elements. In the meantime, the PSE and THI were shown to have an adverse effect on the system's throughput performance. Recently, an IRS-assisted NLEH scheme was proposed with the help of IRS in the downlink WET so as to enable the IRS-assisted uplink WIT [21], where the fractional energy harvesting model was transformed to a subtractive form to derive IRS beam patterns and time allocations. In [22], the potential of IRS was unlocked in an full-duplex WPCN (FD-WPCN), where an H-AP simultaneously radiated energy signals in downlink WET and received information signal in uplink WIT. Full dynamic IRS beam pattern was optimally designed with transmission time allocation, and outperformed the partially dynamic and static IRS beam patterns, which mitigated signalling overhead and implementation complexity. The IRS-assisted FD WPCN was further extended to the MIMO scenario, and particularly, the weighted sum throughput was maximised, which was solved by the element-wise (EW) based algorithm to design the optimal IRS beam patterns [23]. Several recent state-of-the-art papers have explored the IRS-assisted WPCN in various contexts [24]–[28]. The work in [24] investigated a double-IRS-assisted wireless powered NOMA network to improve the downlink WET and uplink WIT. In [25], secrecy performances of the IRS-assisted WPCN in terms of connection outage probability (COP), secrecy outage probability (SOP) and effective secrecy performance (ESP), were theoretically analyzed in three different models, i.e., co-located AP, and two separated PS and AP cases with different deployments of IRS. In [26], the authors first proposed an IRS-assisted wireless powered heterogeneous network (WPHN), containing two types of IoT devices, i.e., energy-harvesting devices (EHD) and non-energy-harvesting devices (NEHD), and utilizing IRS to improve downlink WET for the EHD and uplink WIT for the EHDs and NEHDs. The IRS-assisted wireless powered secure mobile edge computing (WP-SMEC) network was presented in [27] to explore the trade-off between the WET efficiency, secure computational offloading and local computing. In [28], a Stackleberg game-based multiple access scheme has been designed in an IRS-assisted WPCN, which fits with the case that both downlink WET and uplink WIT networks belong to different service suppliers and thus IoT devices need to provide monetary payment in exchange for the wireless charging of the PS.

Although the aforementioned works focus on the IRS-assisted WPCN, the multi-antenna AP that employs receive beamforming to decode the information from multiple devices at the uplink WIT has not been fully exploited. On the other hand, it is imperative to exploit the downlink and uplink IRS beam patterns in the WPCN to demonstrate the advantage of IRS to enable the energy harvesting and information transmission capabilities. Moreover, there is a paucity of work

that investigates the joint optimisation of energy beamforming, receive beamforming, as well as downlink and uplink IRS beam patterns in the IRS-assisted WPCN with multi-antenna PS and AP.

In this context, this work investigates an IRS-aided WPCN in which a multi-antenna equipped PS uses energy beamforming to wirelessly charge IoT devices in the downlink WET, thereby harvesting energy to support their data transmission in the uplink WIT. In [29], an IRS-assisted WPCN with a separate energy/information transceiver was considered, where multiple IoT devices collect energy from a multi-antenna PS with the help of IRS and then transmit their signals to the AP wirelessly using the harvested energy. An energy efficiency (EE) maximization problem was formulated in [29], which aimed to evaluate the impact of energy consumption on overall performance and guarantee the quality of service (QoS) of each IoT device. Note that our work differs from those in the literature from two aspects. First, the direct link between PS and IoT devices is completely blocked by obstacles; Second, IRS only participates in the downlink WET downlink to support the energy harvesting from PS to IoT devices, while the IRS has no influence on the uplink WIT. In [30], a PS provided wireless charging for an AP to support its downlink WIT with NOMA, and the IRS was deployed to improve the energy harvesting and information transmission capabilities. Although this work examined the IRS involvement in WIT and WET and considered a sum throughput maximization problem, it is still significantly different from our work. Specifically, our work presents an IRS-assisted downlink WET and uplink WIT. In the downlink WET, the IRS assists the PS to wirelessly charge the IoT devices using energy beamforming. Then, these devices simultaneously transmit their individual information to the AP, which uses multi-user decomposition (MUD) technology to restore the information of each device. In addition, the work in [30] considered the power constraint of SIC demodulation and the QoS requirement of each device, since the NOMA scheme was used in the downlink WIT. Regarding the optimization algorithms, in [29], the authors proposed to apply the Dinkelbach's method to recast the fractional EE objective function into the subtractive form for traceability. Then, an AO algorithm was adopted to alternately co-design the solutions for energy beamforming, time scheduling, power allocation, and IRS phase shifts for downlink WET. The Lagrange dual method with subgradient method was considered to iteratively derive the semi-closed-form solutions for energy beamforming, time scheduling, power allocation for given IRS phase shifts, which is then numerically solved by the semidefinite programming (SDP). In [30], the AO and SCA algorithms was presented to solve the formulated problem. Compared with the existing studies, e.g., [29] and [30], *the system model and algorithm design in our work generate unique contributions, the most important of which are summarised as follows:*

1) The considered system model includes two time intervals or phases, one for downlink WET and the other for uplink WIT. In the downlink WET phase, the IoT devices collect the RF energy radiated from the multi-antenna PS, and then utilise the harvested energy to transmit their own information in the uplink WIT phase. The multi-antenna AP employs receive beamforming to decode the information signal of each device. Unlike [29] and [30], our work focuses on the sum throughput maximization problem, where the sum throughput is maximized to enhance the total network performance, subject to the energy consumption constraint of each IoT device, time scheduling, energy beamforming, as well as IRS phase shifts for downlink WET and uplink WIT. The formulated non-convex problem includes multiple coupled variables, i.e., energy/received beamforming, IRS phase shifts, power allocation, and time scheduling.
2) In this work, a two-level method for decomposing the formulated problem is proposed, which has a novel design compared to [29] and [30]. For the outer level, it is a single-variable optimization problem with respect to time scheduling. By fixing energy/receive beamforming, IRS phase shifts, and power allocation, we numerically search for optimal time scheduling using a one-dimensional (1-D) line method. For the inner level, a block coordinate descent (BCD) iterative algorithm is applied to optimize the receive beamforming, power allocation, energy beamforming, and IRS phase shifts in an alternating manner. In particular, the MSE is minimised accordingly to derive the closed-form expression for the receive beamforming. In addition, the Lagrange dual transformation (LDT), quadratic transformation (QT), and alternating direction method of multipliers (ADMM) are proposed to iteratively design the optimal solutions for energy beamforming, and power allocation, and IRS phase shifts.
3) This work also provides comprehensive simulation results to validate the theoretical derivations and performance gains of the proposed algorithm. Specifically, the numerical searches, i.e., the 1-D and golden methods, can achieve an identical optimal solution for time scheduling. The convergence of the proposed algorithm is also effectively verified. In addition, the number of IRS reflecting element, the transmit power of PS, and the number of PS and AP, can be increased to enhance the sum throughput performance. Furthermore, the proposed algorithm has a significant superiority over the benchmark schemes, and the results show that the increase of IRS reflecting elements saves the WET scheduling time without sacrificing the sum harvested energy.

The remaining part of this paper is organised as follows: the system model and problem formulation are depicted in Section II, and the formulated problem is solved in Section III; numerical results are presented in Section IV to validate the theoretical derivations, and Section V concludes the paper.

II. System Model and Problem Formulation

An IRS-empowered WPCN structure is depicted in Fig. 1, where a PS, comprise of multiple antennas, utilises energy beamforming to broadcast RF energy to K IoT devices (i.e., $\mathcal{D}_k, \ \forall k \in \{1, ..., K\}$) in the downlink WET, which then use harvested energy to support information transmission in

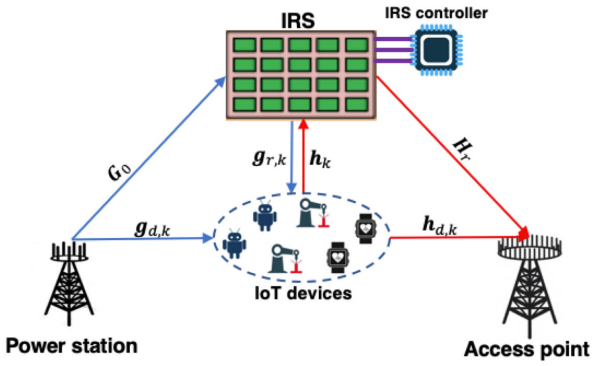

Fig. 1: System model.

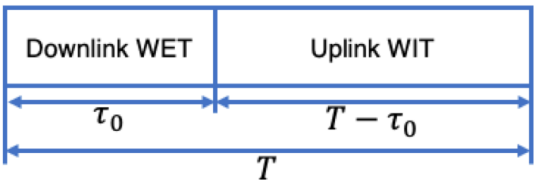

Fig. 2: The transmission structure.

the uplink WIT. An AP is equipped with multiple antennas, aiming to recover data of each device by exploiting the MUD technique. Meanwhile, an IRS aims to participate in the downlink WET and uplink WIT so as to bring the energy harvesting and data transmission performance gains by generating passive beam patterns. The PS, AP, and IRS are equipped with N_T transmitting antennas and N_A receiving antennas, and N_R passive reflecting elements, respectively. In our work, we mainly focus on developing optimization strategies suitable for the IRS-assisted WPCN with multi-antenna PS and AP, and we are interested in the upper bounds of the sum throughput performance for the considered system model, for which the perfect channel state information (CSI) is in general assumed. To address the imperfect CSI issue of IRS-assisted wireless networks, there has been channel estimation techniques and CSI uncertainties or channel estimation errors modelled in the existing works [31]–[34]. As expected, the channel estimation techniques and CSI uncertainties or channel estimation errors will lead to sum throughput performance degradation, which can be tackled by using robust resource allocations for active transmit beamforming and IRS reflecting coefficients. We assumes block-fading, e.g., the channel remains static within one time block but may change at the next time block. The channel coefficients for PS-$\mathcal{D}_k$, PS-IRS, IRS-$\mathcal{D}_k$, $\mathcal{D}_k$-AP, $\mathcal{D}_k$-IRS, and IRS-AP links are represented by $\mathbf{g}_{d,k} \in \mathbb{C}^{N_T\times 1}$, $\mathbf{G}_0 \in \mathbb{C}^{N_R\times N_T}$, $\mathbf{g}_{r,k} \in \mathbb{C}^{N_R\times 1}$, $\mathbf{h}_{d,k} \in \mathbb{C}^{N_A\times 1}$, $\mathbf{h}_k \in \mathbb{C}^{N_R\times 1}$, and $\mathbf{H}_r \in \mathbb{C}^{N_A\times N_R}$, respectively. As shown in Fig. 2, we denote the whole time duration as T, where the IoT devices collect energy at the downlink WET time period of $\tau_0 \in [0, T]$, and they simultaneously transmit information to the AP at the uplink WIT time slot of $T-\tau_0$. Moreover, the IRS passive reflecting coefficients for downlink WET and uplink WIT are denoted by $\mathbf{\Theta}_m = \text{diag}\left[\theta_{m,1}, ..., \theta_{m,N_R}\right], \quad \forall m \in \{0,1\}, \quad \forall n \in \{1, ..., N_R\}$, where each element $\theta_{m,n} = \beta_{m,n}\exp(j\alpha_{m,n})$ is the associated reflecting coefficient that is composed of amplitude $\beta_{m,n} \in [0,1]$ and phase $\alpha_{m,n} \in [0, 2\pi)$.[1] Denote $\mathbf{w} \in \mathbb{C}^{N_T\times 1}$ as the coefficients for energy beamforming by the PS, which satisfies $|\mathbf{w}|^2 = 1$. At the downlink WET time duration of τ_0, the harvested energy at $\mathcal{D}_k$, $\forall k \in \{1, ..., K\}$ is given by

$$E_k = \tau_0 \min\left(\eta_k P_0 \left|\left(\mathbf{g}_{r,k}^H \mathbf{\Theta}_0 \mathbf{G}_0 + \mathbf{g}_{d,k}^H\right)\mathbf{w}\right|^2, P_s\right), \quad (1)$$

where $\eta_k \in (0,1]$, $\forall k \in \{1, ..., K\}$ is the energy harvesting efficiency in the linear region; P_s represents the saturation power, and the harvested power will not increase beyond this threshold. Equation (1) has two terms, where the first one follows the LEH model with an energy conversion efficiency η_k to approximately linearise the practical non-linear harvester; the second term is a saturated threshold of the harvested power, which means that the harvested power first linearly increases in terms of the received power as seen in the first term of (1), and then gradually approaches the saturated threshold P_s denoted by the second term in (1). Suppose that the harvested power at each device does not exceed the threshold P_s. Then, at the uplink WIT time period of $T-\tau_0$, the received signal at the AP is given by

$$\mathbf{y}^{UL} = \sum_{k=1}^{K} \sqrt{p_k}\left(\mathbf{H}_r \mathbf{\Theta}_1 \mathbf{h}_k + \mathbf{h}_{d,k}\right) x_k^{UL} + \mathbf{n}, \quad (2)$$

where $p_k = \frac{E_k}{T-\tau_0}$ and $x_k^{UL} \in \mathbb{C}$ are the transmit power and symbol of $\mathcal{D}_k$, respectively; $\mathbf{n}$ is the noise vector at the AP. Here, we consider the MUD technique to recover each IoT devices signal, where $\mathbf{F} \in \mathbb{C}^{N_A\times K} = [\mathbf{f}_1, ..., \mathbf{f}_K]$ is adopted, and $\mathbf{f}_k \in \mathbb{C}^{N_A\times 1}$ is denoted by the k-th column of $\mathbf{F}$ for recovering of $\mathcal{D}_k$. Via MUD, the signal of $\mathcal{D}_k$ decoded by the AP can be expressed as

$$\begin{aligned}\tilde{x}_k^{UL} &= \mathbf{f}_k^H \mathbf{y}^{UL} \\ &= \mathbf{f}_k^H \left(\sum_{j=1}^{K} \sqrt{p_j}\left(\mathbf{H}_r \mathbf{\Theta}_1 \mathbf{h}_j + \mathbf{h}_{d,j}\right) x_j^{UL} + \mathbf{n}\right). \quad (3)\end{aligned}$$

Thus, the individual throughput at the AP decoding the information from $\mathcal{D}_k$ is given at (4) on the top of the next page, where σ^2 is the noise power of the AP. We proceed to maximise the sum throughput, with the constraints of IoT device's transmit power, IRS phase shifts, energy beamfoming of PS, and time allocation. Thus, this problem is formulated as (5) on the top of the next page, where $\mathbf{\Theta} = [\mathbf{\Theta}_0, \mathbf{\Theta}_1]$, and $\mathbf{p} = [p_1, ..., p_K]$. Problem (5) is non-convex due to its objective function (5a), as well as constraints (5b) and (5c), which cannot be solved directly.

[1] In our work, the amplitude is typically set to be one, which aims to maximize the reflected signal. Hence, the IRS reflecting coefficients can be written as $|\theta_{m,n}| = \beta_{m,n} = 1$.

$$R_k = (T-\tau_0)\log\left(1+\frac{p_k\left|\mathbf{f}_k^H\left(\mathbf{H}_r\boldsymbol{\Theta}_1\mathbf{h}_k+\mathbf{h}_{d,k}\right)\right|^2}{\sum_{j\neq k}p_j\left|\mathbf{f}_k^H\left(\mathbf{H}_r\boldsymbol{\Theta}_1\mathbf{h}_j+\mathbf{h}_{d,j}\right)\right|^2+\sigma^2\mathbf{f}_k^H\mathbf{f}_k}\right). \tag{4}$$

$$\max_{\mathbf{w},\mathbf{F},\boldsymbol{\Theta},\mathbf{p},\tau_0} \sum_{k=1}^{K}(T-\tau_0)\log\left(1+\frac{p_k\left|\mathbf{f}_k^H\left(\mathbf{H}_r\boldsymbol{\Theta}_1\mathbf{h}_k+\mathbf{h}_{d,k}\right)\right|^2}{\sum_{j\neq k}p_j\left|\mathbf{f}_k^H\left(\mathbf{H}_r\boldsymbol{\Theta}_1\mathbf{h}_j+\mathbf{h}_{d,j}\right)\right|^2+\sigma^2\mathbf{f}_k^H\mathbf{f}_k}\right), \tag{5a}$$

$$s.t.\ (T-\tau_0)p_k \le \tau_0\eta_k P_0\left|\left(\mathbf{g}_{r,k}^H\boldsymbol{\Theta}_0\mathbf{G}_0+\mathbf{g}_{d,k}^H\right)\mathbf{w}\right|^2,\ \forall k\in\{1,...,K\}, \tag{5b}$$

$$|\theta_{m,n}|=1,\ \forall m\in\{0,1\},\ \forall n\in\{1,...,N_R\}, \tag{5c}$$

$$0\le\tau_0\le T, \tag{5d}$$

$$|\mathbf{w}|^2\le 1. \tag{5e}$$

III. Optimal Solution of Problem (5)

To find the optimal solutions for energy beamforming $\mathbf{w}$, transmit power of IoT devices $\mathbf{p}$, receive beamforming $\mathbf{F}$ at the AP, IRS phase shifts $\boldsymbol{\theta}$, and time scheduling τ_0, first, we perform the following mathematical manipulations:

$$t_{0,k}=\left|\left(\mathbf{g}_{r,k}^H\boldsymbol{\Theta}_0\mathbf{G}_0+\mathbf{g}_{d,k}\right)\mathbf{w}\right|^2=\left|\left(\boldsymbol{\theta}_0^H\mathbf{A}_k+\mathbf{g}_{d,k}^H\right)\mathbf{w}\right|^2, \tag{6a}$$

$$t_{1,k,j}=\left|\mathbf{f}_k^H\left(\mathbf{H}_r\boldsymbol{\Theta}_1\mathbf{h}_j+\mathbf{h}_{d,j}\right)\right|^2=\left|\mathbf{f}_k^H\left(\mathbf{B}_j\boldsymbol{\theta}_1+\mathbf{h}_{d,j}\right)\right|^2, \tag{6b}$$

where $\boldsymbol{\theta}=\{\boldsymbol{\theta}_m\}_{m=0}^1$, $\boldsymbol{\theta}_m=[\theta_{m,1},...,\theta_{m,N}]^T$, $\mathbf{A}_k=\text{diag}\left(\mathbf{g}_{r,k}^H\right)\mathbf{G}_0$, and $\mathbf{B}_k=\mathbf{H}_r\text{diag}\left(\mathbf{h}_k\right)$. With (6a) and (6b), problem (5) is equivalent to

$$\max_{\mathbf{w},\mathbf{F},\boldsymbol{\theta},\mathbf{p},\tau_0}\ (T-\tau_0)\sum_{k=1}^{K}\log\left(1+\frac{p_k t_{1,k,k}}{\sum_{j\neq k}p_j t_{1,k,j}+\sigma^2\mathbf{f}_k^H\mathbf{f}_k}\right), \tag{7a}$$

$$s.t.\ (T-\tau_0)p_k\le\tau_0\eta_k P_0 t_{0,k},\ \forall k\in\{1,...,K\}, \tag{7b}$$

$$\text{(5c), (5d), (5e).} \tag{7c}$$

To solve (7), we propose a two-level method. Specifically, we first fix $\mathbf{w}$, $\mathbf{p}$, $\mathbf{F}$, and $\boldsymbol{\theta}$ to optimize the transmission time scheduling τ_0, where its optimal solution can be numerically searched via the 1-D line method. In the following, we solve the inner level problem for a given τ_0, by applying a BCD iterative algorithm to alternately design $\mathbf{F}$, $\mathbf{w}$, $\mathbf{p}$, and $\boldsymbol{\theta}$.

A. Optimal Solution of $\mathbf{F}$

In this subsection, we fix $\mathbf{w}$, $\boldsymbol{\theta}$, and $\mathbf{p}$ to optimize $\mathbf{F}$. Denote $\mathbf{d}_k=\mathbf{B}_k\boldsymbol{\theta}_1+\mathbf{h}_{d,k}$, and (7) is written in terms of $\mathbf{F}$, as

$$\max_{\mathbf{F}}\ \sum_{k=1}^{K}\log\left(1+\frac{p_k\left|\mathbf{f}_k^H\mathbf{d}_k\right|^2}{\sum_{j\neq k}p_j\left|\mathbf{f}_k^H\mathbf{d}_j\right|^2+\sigma^2\mathbf{f}_k^H\mathbf{f}_k}\right). \tag{8}$$

The closed-form solution for $\mathbf{f}_k,\ \forall k\in\{1,...,K\}$, is provided in the following *theorem*,

Theorem 1: For given $\mathbf{w}$, $\boldsymbol{\theta}$, and $\mathbf{p}$, the optimal solution of $\mathbf{f}_k$ is given by

$$\mathbf{f}_k^*=\left(\sum_{j=1}^{K}p_j\mathbf{d}_j\mathbf{d}_j^H+\sigma^2\mathbf{I}_{N_A\times N_A}\right)^{-1}\sqrt{p_k}\mathbf{d}_k. \tag{9}$$

Proof: Note that (8) is equivalent to the individual throughput maximization with respect to $\mathbf{F}$ due to the independence of R_k in (4) with respect to $\mathbf{f}_k$. Thus, (8) is further written as

$$\max_{\mathbf{F}}\ \log\left(1+\frac{p_k\left|\mathbf{f}_k^H\mathbf{d}_k\right|^2}{\sum_{j\neq k}p_j\left|\mathbf{f}_k^H\mathbf{d}_j\right|^2+\sigma^2\mathbf{f}_k^H\mathbf{f}_k}\right). \tag{10}$$

Next, the maximization of (10) is equivalent to the minimization of MSE, as

$$\begin{aligned}\min_{\mathbf{F}}\ \text{MSE}_k\ &=\mathbb{E}\left(\hat{x}_k^{UL}-x_k^{UL}\right)^2\\ &=\mathbb{E}\left[x_k^{UL}-\mathbf{f}_k\left(\sum_{j=1}^{K}\sqrt{p_j}\mathbf{d}_j x_j+\mathbf{n}\right)\right]^2.\end{aligned} \tag{11}$$

As the transmit-symbol guarantees that $\mathbb{E}\left(\left(x_k^{UL}\right)^2\right)=1$ and $\mathbb{E}\left(x_k^{UL}x_j^{UL}\right)=0,\ \forall j\neq k$, (11) is further expanded as

$$\min_{\mathbf{F}}\ \text{MSE}_k=1-2\sqrt{p_k}\mathbf{f}_k^H\mathbf{d}_k+\left(\mathbf{f}_k^H\sum_{j=1}^{K}\sqrt{p_j}\mathbf{d}_j\right)^2+\sigma^2\mathbf{f}_k^H\mathbf{f}_k. \tag{12}$$

Considering the first-order derivative of (12) with respect to $\mathbf{f}_k$ and setting it to zero, yields

$$\begin{aligned}\frac{\partial\text{MSE}}{\partial\mathbf{f}_k}=0\Rightarrow&\left(\sum_{j=1}^{K}p_j\mathbf{d}_j\mathbf{d}_j^H+\sigma^2\mathbf{I}_{N_A\times N_A}\right)\mathbf{f}_k=\sqrt{p_k}\mathbf{d}_k\\ \Rightarrow\mathbf{f}_k^*=&\left(\sum_{j=1}^{K}p_j\mathbf{d}_j\mathbf{d}_j^H+\sigma^2\mathbf{I}_{N_A\times N_A}\right)^{-1}\sqrt{p_k}\mathbf{d}_k,\end{aligned} \tag{13}$$

which completes the proof of *Theorem* 1. ■

B. Optimal Solution of $\boldsymbol{\theta}_1$

Next, we fix $\mathbf{w}$, $\boldsymbol{\theta}_0$, $\mathbf{p}$, and $\mathbf{F}$, to optimize $\boldsymbol{\theta}_1$. To proceed, problem (7) is expressed with $\boldsymbol{\theta}_1$, as

$$\max_{\boldsymbol{\theta}_1} \sum_{k=1}^{K} \log\left(1+\frac{p_k\left|\mathbf{f}_k^H\left(\mathbf{B}_k\boldsymbol{\theta}_1+\mathbf{h}_{d,k}\right)\right|^2}{\sum_{j\neq k}p_j\left|\mathbf{f}_k^H\left(\mathbf{B}_j\boldsymbol{\theta}_1+\mathbf{h}_{d,j}\right)\right|^2+\sigma^2\mathbf{f}_k^H\mathbf{f}_k}\right), \tag{14a}$$

$$s.t.\ \ |\theta_{1,n}|=1,\ \forall n\in\{1,...,N_R\}. \tag{14b}$$

Due to the fractional property of (14a) and non-convex unit-modulus constraint (14b), (14) is a non-convex problem and cannot be solved directly. To solve it, we propose to utilise the LDT. Denote $X_k = p_k\left|\mathbf{f}_k^H\left(\mathbf{B}_k\boldsymbol{\theta}_1+\mathbf{h}_{d,k}\right)\right|^2$ and $Y_k=\sum_{j\neq k}p_j\left|\mathbf{f}_k^H\left(\mathbf{B}_j\boldsymbol{\theta}_1+\mathbf{h}_{d,j}\right)\right|^2+\sigma^2\mathbf{f}_k^H\mathbf{f}_k$, problem (14) is equivalent to

$$\max_{\boldsymbol{\theta}_1}\ f_0(\boldsymbol{\theta}_1,\mathbf{r})=\sum_{k=1}^{K}\log\left(1+r_k\right)-\sum_{k=1}^{K}r_k+\sum_{k=1}^{K}\frac{(1+r_k)X_k}{X_k+Y_k},$$
$$s.t.\ \text{(14b)}, \tag{15}$$

where $\mathbf{r}=[r_1,...,r_K]^T$ is an auxiliary vector introduced by the LDT. Setting $\frac{\partial f_0}{\partial r_k}=0$, the optimal r_k is derived for given $\boldsymbol{\theta}_1$ as

$$r_k^*=\frac{X_k}{Y_k},\ \forall k\in\{1,...,K\}. \tag{16}$$

For given r_k, (15) is further modified as

$$\max_{\boldsymbol{\theta}_1}\sum_{k=1}^{K}\frac{(1+r_k)p_k\left|\mathbf{f}_k^H\left(\mathbf{B}_k\boldsymbol{\theta}_1+\mathbf{h}_{d,k}\right)\right|^2}{\sum_{j=1}^{K}p_j\left|\mathbf{f}_k^H\left(\mathbf{B}_j\boldsymbol{\theta}_1+\mathbf{h}_{d,j}\right)\right|^2+\sigma^2\mathbf{f}_k^H\mathbf{f}_k}$$
$$s.t.\ \text{(14b)}. \tag{17}$$

Problem (17) is still intractable due to the sum of fractional objective functions. As such, QT is utilised, which aims to recast the sum in (17) into a subtractive form by introducing an auxiliary vector $\boldsymbol{\xi}=[\xi_1,...,\xi_K]^T$. With $\tilde{\mathbf{b}}_{k,j}=\mathbf{f}_k^H\mathbf{B}_j$, and $\hat{b}_{k,j}=\mathbf{f}_k^H\mathbf{h}_{d,j}$, problem (17) is recast as

$$\max_{\boldsymbol{\theta}_1,\boldsymbol{\xi}}\ \sum_{k=1}^{K}2\left[(1+r_k)p_k\right]^{\frac{1}{2}}\Re\left\{\text{conj}\left(\xi_k\right)\tilde{\mathbf{b}}_{k,k}\boldsymbol{\theta}_1+\text{conj}\left(\xi_k\right)\hat{b}_{k,k}\right\}$$
$$-\left|\xi_k\right|^2\left(\sum_{j=1}^{K}p_j\left|\tilde{\mathbf{b}}_{k,j}\boldsymbol{\theta}_1+\hat{b}_{k,j}\right|^2+\sigma^2\mathbf{f}_k^H\mathbf{f}_k\right),$$
$$s.t.\ \text{(14b)}. \tag{18}$$

Problem (18) is still non-convex due to the coupled variables $\boldsymbol{\theta}_1$ and $\boldsymbol{\xi}$, which can be solved in an alternated manner to iteratively update these two variables. First, we fix $\boldsymbol{\theta}_1$ and then use the Lagrange dual method to derive the optimal solution of $\boldsymbol{\xi}$ as

$$\xi_k^*=\frac{\left[(1+r_k)p_k\right]^{\frac{1}{2}}(\tilde{\mathbf{b}}_{k,k}\boldsymbol{\theta}_1+\hat{b}_{k,k})}{\sum_{j=1}^{K}p_j\left|\tilde{\mathbf{b}}_{k,j}\boldsymbol{\theta}_1+\hat{b}_{k,j}\right|^2+\sigma^2\mathbf{f}_k^H\mathbf{f}_k}. \tag{19}$$

Then, (18) is reformulated into the following problem for given ξ_k, as

$$\min_{\boldsymbol{\theta}_1}\ \boldsymbol{\theta}_1^H\boldsymbol{\Omega}_1\boldsymbol{\theta}_1-2\Re\left\{\boldsymbol{\theta}_1^H\boldsymbol{\gamma}_1\right\}$$
$$s.t.\ \ |\theta_{1,n}|=1,\ \forall n\in\{1,...,N_R\}. \tag{20}$$

where

$$\boldsymbol{\Omega}_1=\left(\sum_{k=1}^{K}\xi_k\sum_{j=1}^{K}\tilde{\mathbf{b}}_{k,j}\tilde{\mathbf{b}}_{k,j}^H\right),$$
$$\boldsymbol{\gamma}_1=\sum_{k=1}^{K}2\left[(1+r_k)\,p_k\right]^{\frac{1}{2}}\xi_k\tilde{\mathbf{b}}_{k,k}^H-\sum_{k=1}^{K}\left|\xi_k\right|^2\sum_{j=1}^{K}p_j\hat{b}_{k,j}\tilde{\mathbf{b}}_{k,j}^H.$$

In (20), the constant term in (20) has been omitted for simiplicity. Non-convexity of the unit-modulus constraint leads to the intractability of problem (20). In order to tackle (20), ADMM is applied to derive the closed-form solution of $\boldsymbol{\theta}_1$ iteratively. To proceed, we first introduce a new vector $\boldsymbol{\varrho}\in\mathbb{C}^{N\times1}$ into (20), guaranteeing $\boldsymbol{\varrho}=\boldsymbol{\theta}_1$, which is further modified as

$$\min_{\boldsymbol{\theta}_1,\boldsymbol{\varrho}}\ \boldsymbol{\varrho}^H\boldsymbol{\Omega}_1\boldsymbol{\varrho}-2\Re\left\{\boldsymbol{\varrho}^H\boldsymbol{\gamma}_1\right\}, \tag{21a}$$
$$s.t.\ \ |\theta_{1,n}|=1,\ \forall n\in\{1,...,N_R\}, \tag{21b}$$
$$\boldsymbol{\varrho}=\boldsymbol{\theta}_1. \tag{21c}$$

Consequently, the augmented Lagrange dual function of (21) is applied as

$$\mathcal{L}\left(\boldsymbol{\varrho},\boldsymbol{\theta}_1,\boldsymbol{\chi}\right)=\boldsymbol{\varrho}^H\boldsymbol{\Omega}_1\boldsymbol{\varrho}-2\Re\left\{\boldsymbol{\varrho}^H\boldsymbol{\gamma}_1\right\}-\Re\left\{\boldsymbol{\chi}^H\left(\boldsymbol{\varrho}-\boldsymbol{\theta}_1\right)\right\}$$
$$+\frac{\psi}{2}\left\|\boldsymbol{\varrho}-\boldsymbol{\theta}_1\right\|^2, \tag{22}$$

where $\boldsymbol{\chi}\in\mathbb{C}^{N\times1}$ and $\psi>0$ are the dual vector for constraint (21c) and the penalty factor, respectively. In the following, we proceed to iteratively update $\boldsymbol{\varrho}$, $\boldsymbol{\theta}_1$, and $\boldsymbol{\chi}$. Denote $\boldsymbol{\varrho}^{(i)}$, $\boldsymbol{\theta}_1^{(i)}$, and $\boldsymbol{\chi}^{(i)}$ as the feasible solutions at the i-th iteration.

Update $\boldsymbol{\varrho}^{(i+1)}$: The following sub-problem is explored to update $\boldsymbol{\varrho}^{(i+1)}$,

$$\boldsymbol{\varrho}^{(i+1)}=\arg\min_{\boldsymbol{\varrho}}\mathcal{L}\left(\boldsymbol{\varrho},\boldsymbol{\theta}_1^{(i)},\boldsymbol{\chi}^{(i)}\right). \tag{23}$$

To solve (23), we set the first-order derivative of (23) to zero, as

$$2\boldsymbol{\Omega}_1\boldsymbol{\varrho}^{(i+1)}-2\boldsymbol{\gamma}_1-\boldsymbol{\chi}^{(i)}-\psi\left(\boldsymbol{\theta}_1^{(i)}-\boldsymbol{\varrho}^{(i+1)}\right)=0. \tag{24}$$

With several mathematical manipulations, we have,

$$\boldsymbol{\varrho}^{(i+1)}=\left(\psi\mathbf{I}_N+2\boldsymbol{\Omega}_1\right)^{-1}\left(2\boldsymbol{\gamma}_1+\psi\boldsymbol{\theta}_1^{(i)}+\boldsymbol{\chi}^{(i)}\right). \tag{25}$$

Update $\boldsymbol{\theta}_1^{(i+1)}$: We consider the following sub-problem to update $\boldsymbol{\theta}_1^{(i+1)}$,

$$\boldsymbol{\theta}_1^{(i+1)}=\arg\min_{\boldsymbol{\theta}_1}\ \mathcal{L}\left(\boldsymbol{\varrho}^{(i+1)},\boldsymbol{\theta}_1,\boldsymbol{\chi}^{(i)}\right), \tag{26}$$

which can be equivalently reformulated as

$$\min_{\boldsymbol{\theta}_1}\ \left\|\boldsymbol{\theta}_1-\left(\boldsymbol{\varrho}^{(i+1)}-\frac{1}{\psi}\boldsymbol{\chi}^{(i)}\right)\right\|^2,\ s.t.\ \text{(21b)}. \tag{27}$$

As such, the closed-form solution of (27) is derived as

$$\boldsymbol{\theta}_1^{(i+1)}[n]=\begin{cases}\frac{\left(\boldsymbol{\varrho}^{(i+1)}-\frac{1}{\psi}\boldsymbol{\chi}^{(i)}\right)[n]}{\left|\left(\boldsymbol{\varrho}^{(i+1)}-\frac{1}{\psi}\boldsymbol{\chi}^{(i)}\right)[n]\right|},\ \text{if}\left(\boldsymbol{\varrho}^{(i+1)}-\frac{1}{\psi}\boldsymbol{\chi}^{(i)}\right)[n]\neq0,\\ \boldsymbol{\theta}_1^{(i)}[n],\ \text{otherwise},\end{cases} \tag{28}$$

where $(*)[n]$ denotes the n-th entry of $(*)$.

Update $\boldsymbol{\chi}^{(i)}$: The following equality is utilised to update $\boldsymbol{\chi}$,

$$\boldsymbol{\chi}^{(i+1)} = \boldsymbol{\chi}^{(i)} - \psi \left(\boldsymbol{\varrho}^{(i+1)} - \boldsymbol{\theta}_1^{(i+1)} \right). \tag{29}$$

Substituting (24) into (29) and with some simple manipulations, (29) is equivalent to

$$\boldsymbol{\chi}^{(i+1)} = 2 \left(\boldsymbol{\Omega}_1 \boldsymbol{\varrho}^{(i+1)} - \boldsymbol{\gamma}_1 \right). \tag{30}$$

The following *lemma* is presented for the convergence of the ADMM algorithm,

Lemma 1: The penalty factor ψ satisfies the following condition to guarantee convergence of the ADMM algorithm,

$$\psi \mathbf{I}_{N_R} - \boldsymbol{\Omega}_1 \succ \mathbf{0}. \tag{31}$$

Proof: First, we rewrite (25) as

$$\boldsymbol{\chi}^{(i)} + \psi \boldsymbol{\theta}_1^{(i)} = \left(\psi \mathbf{I}_N + 2\boldsymbol{\Omega}_1 \right) \boldsymbol{\varrho}^{(i+1)} - 2\boldsymbol{\gamma}_1, \tag{32}$$

which is plugged into (29), leading to

$$\begin{aligned} \boldsymbol{\chi}^{(i+1)} &= \boldsymbol{\chi}^{(i)} + \psi \boldsymbol{\theta}_1^{(i)} - \psi \boldsymbol{\varrho}^{(i+1)} \\ &= \left(\psi \mathbf{I}_N + 2\boldsymbol{\Omega}_1 \right) \boldsymbol{\varrho}^{(i+1)} - 2\boldsymbol{\gamma}_1 - \psi \boldsymbol{\varrho}^{(i+1)} \\ &= 2 \left(\boldsymbol{\Omega}_1 \boldsymbol{\varrho}^{(i+1)} - \boldsymbol{\gamma}_1 \right). \end{aligned} \tag{33}$$

Via (33), $\boldsymbol{\chi}$ can be written as a function of $\boldsymbol{\varrho}$,

$$\boldsymbol{\chi} = 2 \left(\boldsymbol{\Omega}_1 \boldsymbol{\varrho} - \boldsymbol{\gamma}_1 \right). \tag{34}$$

Substitute (34) into (22), we obtain (35) on the top of the next page. It can be seen from (35) that the ADMM procedures (23), (26), and (29) are equivalent to the following coordinate ascent problems,

$$\boldsymbol{\varrho}^{(i+1)} = \arg\min_{\boldsymbol{\varrho}} \tilde{\mathcal{L}}_0 \left(\boldsymbol{\varrho}, \tilde{\boldsymbol{\theta}}_{0,m}^{(i)} \right), \tag{36a}$$

$$\tilde{\boldsymbol{\theta}}_{0,m}^{(i+1)} = \arg\min_{\tilde{\boldsymbol{\theta}}_{0,m}} \tilde{\mathcal{L}}_0 \left(\boldsymbol{\varrho}^{(i+1)}, \tilde{\boldsymbol{\theta}}_{0,m} \right), \tag{36b}$$

which can ensure convergence of the ADMM algorithm. ■

Based on the aforementioned derivations, we summarise the detailed steps of the proposed ADMM in *Algorithm* 1. Its convergence has been widely investigated in the existing works [10], [35], [36].

Algorithm 1: The proposed algorithm to solve (14).

1) **Initialisation**: iteration index i, initial points $\mathbf{r}^{(0)}$, $\boldsymbol{\xi}^{(0)}$, $\boldsymbol{\varrho}^{(0)}$, $\boldsymbol{\theta}_1^{(0)}$, and $\boldsymbol{\chi}^{(0)}$.
2) **Set** the penalty factor $\psi = \upsilon \|\boldsymbol{\Omega}_1\|_2$, where $\upsilon \geq 1$ denotes the minimum integer to guarantee (31) in *Lemma* 1.
3) **Repeat**: at the i-th iteration
   a) **Update** $\boldsymbol{r}^{(i+1)}$ via (16).
   b) **Update** $\boldsymbol{\xi}^{(i+1)}$ via (19).
   c) **Update** $\boldsymbol{\varrho}^{(i+1)}$ via (25).
   d) **Update** $\boldsymbol{\theta}_1^{(i+1)}$ via (28).
   e) **Update** $\boldsymbol{\chi}^{(i+1)}$ via (30).
   f) **Set** $i \leftarrow i+1$ **until** convergence.
4) **Collect** the optimal solutions, $\boldsymbol{\theta}_1^*$, $\boldsymbol{\xi}^*$ and $\boldsymbol{r}^*$.

C. Optimal Solution of $\mathbf{p}$, $\mathbf{w}$, and $\boldsymbol{\theta}_0$

In this subsection, we fix $\boldsymbol{\theta}_1$, $\mathbf{F}$, and τ_0 to optimise $\mathbf{p}$, $\mathbf{w}$, and $\boldsymbol{\theta}_0$. First, it is readily observed from (14a) that it monotonically increases in terms of p_k. As such, the optimal solution of p_k can be obtained when (7b) holds the equality,

$$p_k^* = \frac{\tau_0 \eta_k P_0 \left| \left(\boldsymbol{\theta}_0^H \mathbf{A}_k + \mathbf{g}_{d,k}^H \right) \mathbf{w} \right|^2}{T - \tau_0}. \tag{37}$$

Substituting (37) into (14a), and denoting $t_{1,j} = \left| \mathbf{f}_k^H \left(\mathbf{B}_j \boldsymbol{\theta}_1 + \mathbf{h}_{d,j} \right) \right|^2$, $\forall k, j \in [1, K]$, $k \neq j$, we reformulate the optimization problem (7), in terms of $\boldsymbol{\theta}_0$, as

$$\max_{\boldsymbol{\theta}_0, \mathbf{w}} \sum_{k=1}^{K} \log \left(1 + \frac{S_k \left| \left(\boldsymbol{\theta}_0^H \mathbf{A}_k + \mathbf{g}_{d,k}^H \right) \mathbf{w} \right|^2}{\sum_{j \neq k} S_j \left| \left(\boldsymbol{\theta}_0^H \mathbf{A}_j + \mathbf{g}_{d,j}^H \right) \mathbf{w} \right|^2 + \sigma^2 \mathbf{f}_k^H \mathbf{f}_k} \right), \tag{38a}$$

$$s.t. \ \ |\theta_{0,n}| = 1, \ \forall n \in \{1, ..., N_R\}, , \tag{38b}$$

$$\text{(5e)}. \tag{38c}$$

where $S_j = \frac{\tau_0 \eta_j P_0 t_{1,j}}{T - \tau_0}$. Via the LDT as in Section III-B, problem (14) can be transformed in terms of $\mathbf{w}$, and $\boldsymbol{\theta}_0$ as

$$\begin{aligned} \max_{\boldsymbol{\theta}_1, \mathbf{w}} \ & \sum_{k=1}^{K} \frac{(1 + \tilde{r}_k) S_k \left| \left(\boldsymbol{\theta}_0^H \mathbf{A}_k + \mathbf{g}_{d,k}^H \right) \mathbf{w} \right|^2}{\sum_{j=1}^{K} S_j \left| \left(\boldsymbol{\theta}_0^H \mathbf{A}_j + \mathbf{g}_{d,j}^H \right) \mathbf{w} \right|^2 + \sigma^2 \mathbf{f}_k^H \mathbf{f}_k} \\ s.t. \ & \text{(5e)}, \ \ |\theta_{0,n}| = 1, \ \forall n \in \{1, ..., N_R\}. \end{aligned} \tag{39}$$

Similar to Section III-B, the optimal $\tilde{r}_k$ can be derived for given $\mathbf{w}$ and $\boldsymbol{\theta}_0$, which is given by

$$\tilde{r}_k^* = \frac{S_k \left| \left(\boldsymbol{\theta}_0^H \mathbf{A}_k + \mathbf{g}_{d,k}^H \right) \mathbf{w} \right|^2}{\sum_{j \neq k} S_j \left| \left(\boldsymbol{\theta}_0^H \mathbf{A}_j + \mathbf{g}_{d,j}^H \right) \mathbf{w} \right|^2 + \sigma^2 \mathbf{f}_k^H \mathbf{f}_k}. \tag{40}$$

We proceed to tackle problem (39), which aims to alternately optimise $\mathbf{w}$, and $\boldsymbol{\theta}_0$. Now, we first fix $\boldsymbol{\theta}_0$ to optimise $\mathbf{w}$. Specifically, we introduce an auxiliary variable $\tilde{\xi}_k$, $\forall k \in \{1, ..., K\}$, and QT is adopted to recast the sum of fractional objective functions in problem (39) into the subtractive form such that (39) is modified as

$$\begin{aligned} \max_{\mathbf{w}, \tilde{\xi}_k} \ f_1(\mathbf{w}, \tilde{\xi}_k) = & \sum_{k=1}^{K} 2 \left[(1 + \tilde{r}_k) S_k \right]^{\frac{1}{2}} \Re \left\{ \text{conj} \left(\tilde{\xi}_k \right) \boldsymbol{\theta}_0^H \mathbf{A}_k \mathbf{w} \right\} \\ & + 2 \left[(1 + \tilde{r}_k) S_k \right]^{\frac{1}{2}} \Re \left\{ \text{conj} \left(\tilde{\xi}_k \right) \mathbf{g}_{d,k}^H \mathbf{w} \right\} \\ & - \left| \tilde{\xi}_k \right|^2 \sum_{j=1}^{K} S_j \left| \left(\boldsymbol{\theta}_0^H \mathbf{A}_j + \mathbf{g}_{d,j}^H \right) \mathbf{w} \right|^2 - \left| \tilde{\xi}_k \right|^2 \sigma^2 \mathbf{f}_k^H \mathbf{f}_k, \\ s.t. \ & \text{(5e)}. \end{aligned} \tag{41}$$

To proceed, we fix $\mathbf{w}$ to derive the optimal $\tilde{\xi}_k$, which can be derived in closed-form via setting $\frac{\partial f_1}{\partial \tilde{\xi}_k} = 0$, as

$$\tilde{\xi}_k^* = \frac{\left[(1 + \tilde{r}_k) S_k \right]^{\frac{1}{2}} \left[\left(\boldsymbol{\theta}_0^H \mathbf{A}_k + \mathbf{g}_{d,k}^H \right) \mathbf{w} \right]}{\sum_{j=1}^{K} S_j \left| \left(\boldsymbol{\theta}_0^H \mathbf{A}_j + \mathbf{g}_{d,j}^H \right) \mathbf{w} \right|^2 + \sigma^2 \mathbf{f}_k^H \mathbf{f}_k}. \tag{42}$$

$$\begin{aligned}\mathcal{L}(\boldsymbol{\varrho},\boldsymbol{\theta}_1) &= \boldsymbol{\varrho}^H\boldsymbol{\Omega}_1\boldsymbol{\varrho} - 2\Re\left\{\boldsymbol{\varrho}^H\boldsymbol{\gamma}_1\right\} - \Re\left\{2\left(\boldsymbol{\Omega}_1\boldsymbol{\varrho}-\boldsymbol{\gamma}_1\right)^H\left(\boldsymbol{\varrho}-\boldsymbol{\theta}_1\right)\right\} + \frac{\psi}{2}\left\|\boldsymbol{\varrho}-\boldsymbol{\theta}_1\right\|^2 \\ &= \boldsymbol{\varrho}^H\boldsymbol{\Omega}_1\boldsymbol{\varrho} - 2\Re\left\{\boldsymbol{\varrho}^H\boldsymbol{\gamma}_1\right\} + \frac{\psi}{2}\boldsymbol{\varrho}^H\boldsymbol{\varrho} - \psi\Re\left\{\boldsymbol{\theta}_1^H\boldsymbol{\varrho}\right\} + \frac{\psi}{2}\boldsymbol{\theta}_1^H\boldsymbol{\theta}_1 - 2\Re\left\{\boldsymbol{\varrho}^H\boldsymbol{\Omega}_1\boldsymbol{\varrho}\right\} \\ &\quad + 2\Re\left\{\boldsymbol{\varrho}^H\boldsymbol{\Omega}_1\boldsymbol{\theta}_1\right\} + 2\Re\left\{\boldsymbol{\gamma}_1^H\boldsymbol{\varrho}\right\} - 2\Re\left\{\boldsymbol{\gamma}_1^H\boldsymbol{\theta}_1\right\} \\ &= \boldsymbol{\varrho}\left(\frac{\psi}{2}\mathbf{I}_N - \boldsymbol{\Omega}_1\right)\boldsymbol{\varrho} + \frac{\psi}{2}\boldsymbol{\theta}_1^H\boldsymbol{\theta}_1 - \Re\left\{\psi\boldsymbol{\theta}_1^H\boldsymbol{\varrho} + 2\boldsymbol{\varrho}^H\boldsymbol{\Omega}_1\boldsymbol{\theta}_1 - 2\boldsymbol{\gamma}_1^H\boldsymbol{\theta}_1\right\}. \end{aligned} \tag{35}$$

Then, we fix $\tilde{\xi}_k$ and reformulate problem (41) by manipulating f_1 with respect to $\mathbf{w}$ as

$$\begin{aligned}&\min_{\mathbf{w}}\ \mathbf{w}^H\boldsymbol{\Omega}_2\mathbf{w} - 2\Re\left\{\tilde{\mathbf{g}}^H\mathbf{w}\right\}, \\ &s.t.\ \text{(5e)},\end{aligned} \tag{43}$$

where

$$\begin{aligned}\boldsymbol{\Omega}_2 &= \sum_{k=1}^{K}\left|\tilde{\xi}_k\right|^2\sum_{j=1}^{K}S_j\mathbf{g}_j\mathbf{g}_j^H, \\ \tilde{\mathbf{g}}^H &= \sum_{k=1}^{K}\left[\left(1+\tilde{r}_k\right)S_k\right]^{\frac{1}{2}}\mathbf{g}_k, \\ \mathbf{g}_k^H &= \boldsymbol{\theta}_0^H\mathbf{A}_k + \mathbf{g}_{d,k}^H.\end{aligned}$$

To solve (41), the Lagrange multiplier method is then applied to derive the optimal energy beamforming $\mathbf{w}$ as

$$\mathbf{w}^* = \left(\boldsymbol{\Omega}_2 + \lambda\mathbf{I}_{N_T\times N_T}\right)^{-1}\tilde{\mathbf{g}}^H, \tag{44}$$

where $\lambda \geq 0$ is the dual multiplier with respect to (5e), and its optimal solution can be obtained by bisection search.

Then, we fix $\mathbf{w}$ to optimise $\boldsymbol{\theta}_0$. By introducing an auxiliary variable $\hat{\xi}_k$, we apply the QT to recast the sum in (39) to its subtractive counterpart such that (39) can be written with respect to $\boldsymbol{\theta}_0$ as

$$\begin{aligned}\max_{\boldsymbol{\theta}_0,\hat{\xi}_k}\ f_2(\boldsymbol{\theta}_0,\hat{\xi}_k) = &\sum_{k=1}^{K}2\left[\left(1+\tilde{r}_k\right)S_k\right]^{\frac{1}{2}}\Re\left\{\text{conj}\left(\hat{\xi}_k\right)\boldsymbol{\theta}_0^H\mathbf{A}_k\mathbf{w}\right\} \\ &+ 2\left[\left(1+\tilde{r}_k\right)S_k\right]^{\frac{1}{2}}\Re\left\{\text{conj}\left(\hat{\xi}_k\right)\mathbf{g}_{d,k}^H\mathbf{w}\right\} \\ &- \left|\hat{\xi}_k\right|^2\sum_{j=1}^{K}S_j\left|\left(\boldsymbol{\theta}_0^H\mathbf{A}_j+\mathbf{g}_{d,j}^H\right)\mathbf{w}\right|^2 - \left|\hat{\xi}_k\right|^2\sigma^2\mathbf{f}_k^H\mathbf{f}_k, \\ s.t.\ &\text{(38b)}.\end{aligned} \tag{45}$$

Given $\boldsymbol{\theta}_0$, the optimal solution of $\hat{\xi}_k$ can be derived by the Lagrange multiplier method, as

$$\hat{\xi}_k^* = \frac{\left[\left(1+r_k\right)S_k\right]^{\frac{1}{2}}\left(\boldsymbol{\theta}_0^H\mathbf{a}_k + \hat{g}_k\right)}{\sum_{j=1}^{K}S_j\left|\boldsymbol{\theta}_0^H\mathbf{a}_j + \hat{g}_j^H\right|^2 + \sigma^2\mathbf{f}_k^H\mathbf{f}_k} \tag{46}$$

where $\mathbf{a}_j = \mathbf{A}_j\mathbf{w}$, and $\hat{g}_j = \mathbf{g}_{d,j}^H\mathbf{w},\ \forall j \in [1,K]$. For given $\hat{\xi}_k$, (45) can be reformulated with respect to $\boldsymbol{\theta}_0$ as

$$\begin{aligned}&\min_{\boldsymbol{\theta}_0}\ \boldsymbol{\theta}_0^H\boldsymbol{\Omega}_0\boldsymbol{\theta}_0 - 2\Re\left\{\boldsymbol{\theta}_0^H\boldsymbol{\gamma}_0\right\} \\ &s.t.\ \text{(38b)},\end{aligned} \tag{47}$$

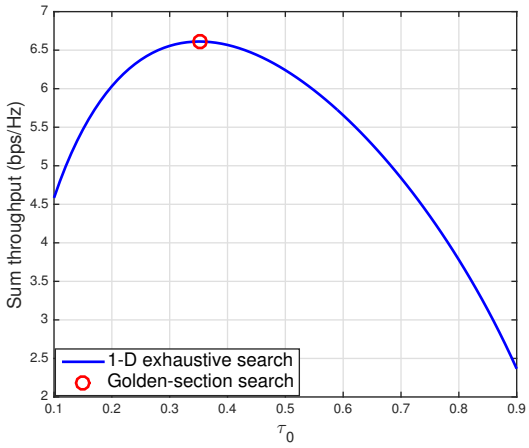

Fig. 3: Comparison between 1-D exhaustive method search and golden search.

where

$$\begin{aligned}\boldsymbol{\Omega}_0 &= \sum_{k=1}^{K}\left|\tilde{\xi}_k\right|^2\sum_{j=1}^{K}S_j\mathbf{a}_j\mathbf{a}_j, \\ \boldsymbol{\gamma}_0 &= \sum_{k=1}^{K}\left[\left(1+r_k\right)S_k\right]^{\frac{1}{2}}\left(\text{conj}\left(\tilde{\xi}_k\right)\mathbf{a}_k\right) \\ &\quad - \sum_{k=1}^{K}\left|\tilde{\xi}_k\right|^2\sum_{j=1}^{K}S_j\text{conj}(\hat{g}_j)\mathbf{a}_j.\end{aligned}$$

The non-convex unit-modulus constraint (38b) leads to intractability of problem (47). To solve it, we employ the ADMM method to derive the optimal solution of $\boldsymbol{\theta}_0$ in an iterative manner, and its procedure has been demonstrated in *Algorithm* 1 of Section III-B and is not repeated here.

D. Overall Algorithm

From the theoretical derivations in Section III-A - III-C, this subsection summarises the overall procedure of the proposed BCD algorithm in *Algorithm* 2.

Algorithm 2: Overall algorithm to solve problem (7).

1) **Fix** τ_0 to iteratively derive the optimal solutions of $\mathbf{F}$, $\mathbf{p}$, $\mathbf{w}$, and $\boldsymbol{\theta}_m,\ \forall m \in \{0,1\}$.
   a) **Initialisation**: iteration index l, initial points $\mathbf{p}^{(0)}$, $\mathbf{w}^{(0)}$, $\boldsymbol{\theta}_m^{(0)},\ \forall m \in \{0,1\}$.
   b) **Repeat**: at the l-th iteration

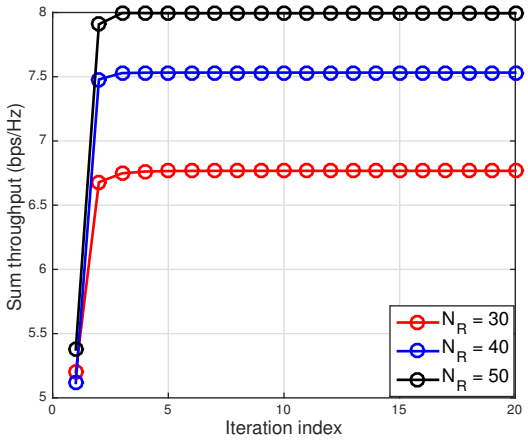

Fig. 4: Convergence performance of *Algorithm* 2.

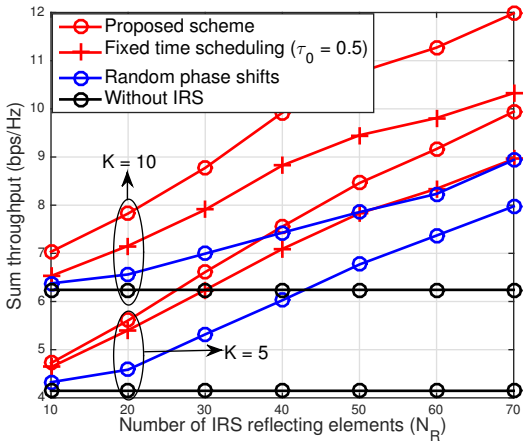

Fig. 5: Sum throughput versus number of IRS reflecting elements N_R.

i) **Fix** $\mathbf{p}^{(l)}$, $\mathbf{w}^{(l)}$, and $\boldsymbol{\theta}_m^{(l)}$ to **update** $\mathbf{F}^{(l+1)}$ via (13).
ii) **Fix** $\mathbf{F}^{(l+1)}$, $\mathbf{p}^{(l)}$, $\mathbf{w}^{(l)}$, and $\boldsymbol{\theta}_0^{(l)}$ to **update** $\boldsymbol{\theta}_1^{(l+1)}$ via *Algorithm* 1.
iii) **Fix** $\mathbf{F}^{(l+1)}$, and $\boldsymbol{\theta}_1^{(l+1)}$ to **update** $\mathbf{p}^{(l+1)}$, $\mathbf{w}^{(l+1)}$, and $\boldsymbol{\theta}_1^{(l+1)}$ via (37), (44), and solving (47) with the ADMM framework. This step is similar to *Algorithm* 1.
iv) **Set** $i \leftarrow i+1$ **until** convergence.

2) **Update** τ_0 by the 1-D line method, i.e., golden search until obtaining its optimal solution, i.e., τ_0^*.
3) **Collect** the optimal solutions, $\mathbf{F}^*$, $\mathbf{p}^*$, $\mathbf{w}^*$, and $\boldsymbol{\theta}_m^*$, $\forall m \in \{0,1\}$.

Now, let us characterize the convergence property of *Algorithm* 2 by the following *lemma*:

Lemma 2: The sum throughput yields a monotonically non-decreasing behaviour over iteration, and the converged solution is a stationary point when *Algorithm* 2 is guaranteed to converge.

Proof: Please see *Appendix* V-A. ■

Then, we proceed to discuss the computational computational complexity of the proposed algorithm (i.e., *Algorithm* 2). We set the maximum iteration numbers to guarantee the convergence of the ADMM algorithm for optimizing the downlink WET/uplink WIT IRS phase shifts, the BCD algorithm, and one-dimensional (1-D) line search (i.e., golden search) as $I_{ADMM,D/U}$, I_{BCD}, and I_G, respectively. First, the computational complexity of received beamforming is given by $\mathcal{O}\left(KN_A^3\right)$. Next, the computational complexity of the energy beamforming is given by $\mathcal{O}\left(N_T^2\right)$. Then, the complexity to optimize the downlink WET/uplink WIT IRS phase shifts is $\mathcal{O}\left(I_(ADMM,q)(N_R^2+KN_R)\right)$, $\forall q = \{D,U\}$. Thus, the computational complexity to implement *Algorithm* 2 is $\mathcal{O}\left\{I_G I_{BCD}[KN_A^3+N_T^2+I_{ADMM,D}(N_R^2+KN_R) +I_{ADMM,U}(N_R^2+KN_R)]\right\}$.

IV. Numerical Results

Here, we provide the numerical results to validate the theoretical derivations presented in Section III, and examine the performance of the system under investigation. In simulations, a three-dimensional (3-D) coordinate is employed to depict the node deployment, in which the coordinates of PS, AP, and IRS are set to $(-15,0,0)$, $(15,0,0)$, and $(-2,6,0)$, respectively. The IoT devices are randomly distributed at an $x-z$ circular area with centre $(0,0)$ and radius 5 metres. All IRS-related and direct channel coefficients are modelled as Rician fading and Rayleigh fading, respectively [15].

$$\begin{aligned}
\mathbf{G}_0 &= \sqrt{\mathcal{PL}_q}\left[\sqrt{\frac{K_1}{K_1+1}}\bar{\mathbf{G}}_0^{\text{LOS}}+\sqrt{\frac{1}{K_1+1}}\bar{\mathbf{G}}_0^{\text{NLOS}}\right],\\
\mathbf{g}_{r,k} &= \sqrt{\mathcal{PL}_q}\left[\sqrt{\frac{K_1}{K_1+1}}\bar{\mathbf{g}}_{r,k}^{\text{LOS}}+\sqrt{\frac{1}{K_1+1}}\bar{\mathbf{g}}_{r,k}^{\text{NLOS}}\right],\\
\mathbf{h}_k &= \mathbf{g}_{r,k}^T,\\
\mathbf{H}_r &= \sqrt{\mathcal{PL}_q}\left[\sqrt{\frac{K_1}{K_1+1}}\bar{\mathbf{H}}_r^{\text{LOS}}+\sqrt{\frac{1}{K_1+1}}\bar{\mathbf{H}}_r^{\text{NLOS}}\right],\\
\mathbf{g}_{d,k} &= \sqrt{\mathcal{PL}_q}\bar{\mathbf{g}}_{d,k},\ \mathbf{h}_{d,k} = \sqrt{\mathcal{PL}_q}\bar{\mathbf{h}}_{d,k},
\end{aligned} \tag{48}$$

where $\bar{\mathbf{G}}_0^{\text{LOS}}$, $\bar{\mathbf{g}}_{r,k}^{\text{LOS}}$, $\bar{\mathbf{H}}_r^{\text{LOS}}$ denote the line-of-sight (LoS) components of the corresponding channels; $\bar{\mathbf{G}}_0^{\text{NLOS}}$, $\bar{\mathbf{g}}_{r,k}^{\text{NLOS}}$, $\bar{\mathbf{H}}_r^{\text{NLOS}}$ are the non-line-of-sight (NLOS) components of the corresponding channels; $\bar{\mathbf{g}}_{d,k}$ and $\bar{\mathbf{h}}_{d,k}$ are zero-mean circularly symmetric independent and identically distributed Gaussian random variables. Following our previous works [12], [15], [20], the path-loss model is denoted as $\mathcal{PL}_q = \mathcal{R}_0\left(\frac{d_q}{d_0}\right)^{\varepsilon_q}$, in which $\mathcal{R}_0 = -30$ dBm, and $d_0 = 1$ metre is the reference distance; d_q and ε_q, $\forall q \in [PS2IRS, IRS2D, PS2D, IRS2AP, D2AP]$ are the distance and path-loss exponent of the PS-IRS, IRS-$\mathcal{D}_k$, PS-$\mathcal{D}_k$, IRS-AP, and $\mathcal{D}_k$-AP links, respectively. The other parameters are set to: $N_T = 6$, $N_R = 30$, $N_A = 5$, $K = 5$, $\sigma^2 = -110$ dBm, $T = 1$ second, $\varepsilon_{PS2IRS} = \varepsilon_{IRS2AP} = 2$, $\varepsilon_{IRS2D} = 2.5$, and $\varepsilon_{PS2D} = \varepsilon_{D2AP} = 3.5$.

First, we verify the correctness of the 1-D exhaustive search over τ_0 in Fig. 3 in comparison to the golden section search, which shows the sum throughput versus the time scheduling τ_0 with both search methods. As seen in this figure, the 1-

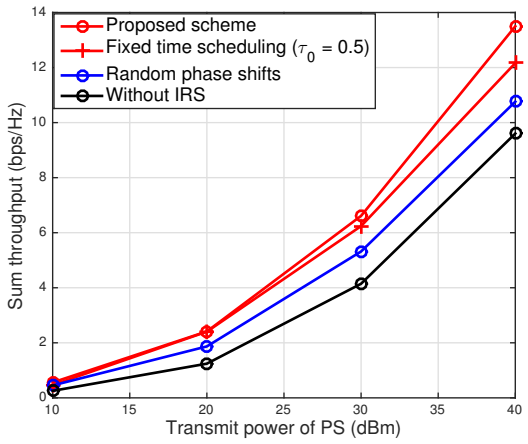

Fig. 6: Sum throughput versus transmit power of PS P_0.

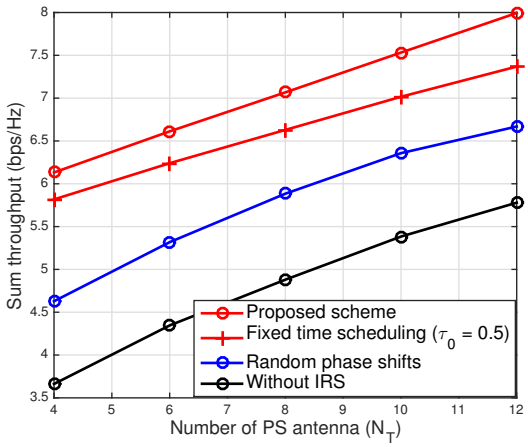

Fig. 7: Sum throughput versus number of PS's transmit antennas N_T.

D exhaustive search demonstrates a concave behaviour with respect to τ_0, and achieves an identical maximum point to that of the golden search method. This highlights the effectiveness of the golden search method due to its low-complexity. As indicated by Fig. 4, the proposed algorithm shows a monotonically increasing behaviour and then converges roughly at the fourth or fifth iteration. This verifies the convergence property of the proposed LDT, QT, and ADMM approaches for alternately performing energy beamforming, power allocation, IRS passive beam patterns, and received beamforming.

Then, we provide the following schemes for comparison with the same setup to highlight the proposed scheme.

1) *Fixed time scheduling*: Energy beamforming, power allocation, IRS phase shifts, receive beamforming are optimally designed with fixed time scheduling $\tau_0 = 0.5$.
2) *Random phase shifts*: Each element of IRS phase shift matrix is randomly generated at $[0, 2\pi]$.
3) *Without IRS*: The system model is reduced to a WPCN without IRS's participation in WET and WIT, where energy beamforming, power allocation, and receive beamforming are jointly optimised by the proposed algorithm.
4) *Majorization-Minimization (MM)-based Algorithm [12]*: The MM-based algorithm is employed to derived the semi-closed-form solution of the downlink WET and uplink WIT IRS phase shifts.
5) *Imperfect CSI case*: Here, the cascaded CSIs of the downlink WET and uplink WIT are considered to be imperfectly available. The actual CSIs can be modelled as $\mathbf{A}_k = \bar{\mathbf{A}}_k + \Delta_{\mathbf{A}_k}$ and $\mathbf{B}_k = \bar{\mathbf{B}}_k + \Delta_{\mathbf{B}_k}$, where $\bar{\mathbf{A}}_k$ and $\bar{\mathbf{B}}_k$ are the estimated cascaded CSI for downlink WET and downlink WIT, respectively [32]. Also, $\Delta_{\mathbf{A}_k}$ and $\Delta_{\mathbf{B}_k}$ denote the corresponding estimation errors, satisfying $\|\Delta_{\mathbf{A}_k}\|_F \leq \delta_{DL,k}$ and $\|\Delta_{\mathbf{B}_k}\|_F \leq \delta_{UL,k}$, where $\delta_{DL,k}$, and $\delta_{UL,k}$ denote the CSI uncertainty bound for the downlink WET and uplink WIT, respectively, and we assume that $\delta_{DL,k} = \delta_{UL,k} = \delta$.

The sum throughput against the number of IRS reflecting elements N_R with different numbers of IoT devices, i.e., $K = 5$ and $K = 10$ is shown in Fig. 5. It can be indicated by this result that the IRS-based schemes, i.e., the proposed scheme, the scheme with fixed time scheduling $\tau_0 = 0.5$, and the random phase shift scheme, exhibit a monotonically increasing trend, significantly outperforming the scheme without IRS. In addition, the proposed scheme has a better sum throughput performance than the fixed time scheduling, the random phase shift, and no IRS counterparts, which highlights the positive impact of the IRS on the uplink WIT in comparison to these benchmark schemes. The advantage of optimal time scheduling design, optimal IRS phase shift design, and IRS employment is manifested by the sum rate performance gain of the proposed scheme. In addition, more IoT devices can bring a larger sum throughput gain, which shows the positive impact of IRS on the uplink WIT, stemming from the fact that more devices utilizing the harvested energy are involved in WIT.

Fig. 6 illustrates the impact of PS's transmit power P_0 on the sum throughput, showing a monotonic growth with respect to P_0 for all schemes. This emphasises that a higher power consumed by the PS can enhance the energy harvesting capability at IoT devices to better support information delivery during WIT, which further confirms the positive impact of IRS on the uplink WIT, especially in the large power region. Additionally, the proposed scheme outperforms its counterparts with fixed time scheduling τ_0 and with random phase shifts, respectively. This highlights a positive impact of optimal time scheduling design and optimal IRS phase shift design on sum throughput performance. Moreover, the employment of IRS is important in the proposed scheme, leading to a significant gain over that without IRS with respect to sum throughput.

The impact of the number of transmit and receiving antennas of the PS and AP N_T and N_A on the sum throughput performance is examined in Fig. 7 and Fig. 8, respectively. In Fig. 7, the proposed scheme has a performance gain over the other benchmark schemes, which monotonically increases with N_T. This result reveals the fact that a larger number of transmit antennas, i.e., N_T, can increase the power consumption at the PS via energy beamforming to enhance energy and further information receptions at the IoT devices and the AP,

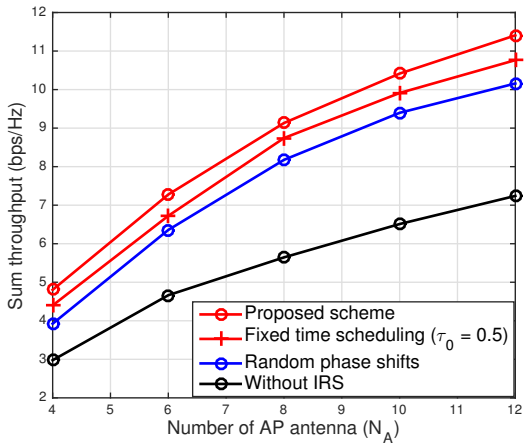

Fig. 8: Sum throughput versus number of AP's receiving antennas N_A.

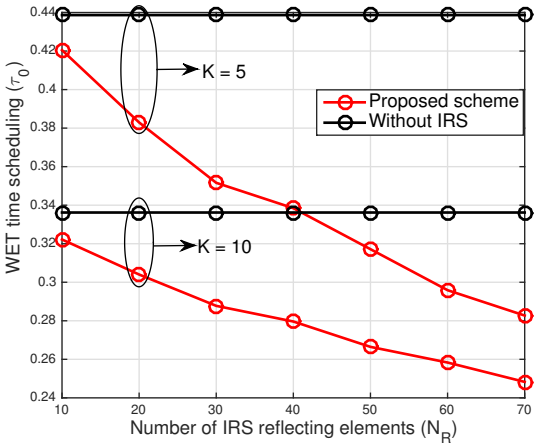

Fig. 10: Optimal WET time scheduling τ_0 versus number of IRS reflecting element N_R.

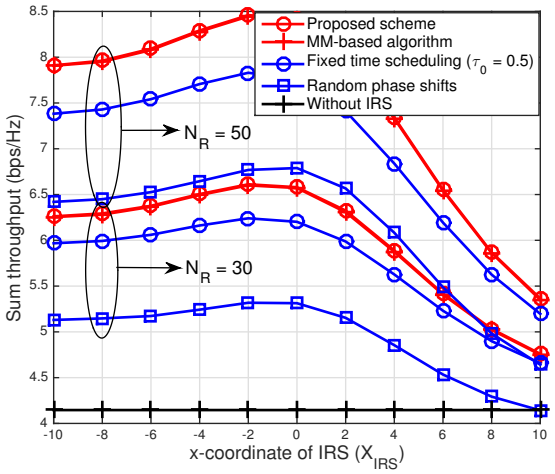

Fig. 9: Sum throughput versus x-coordinate of IRS X_{IRS}.

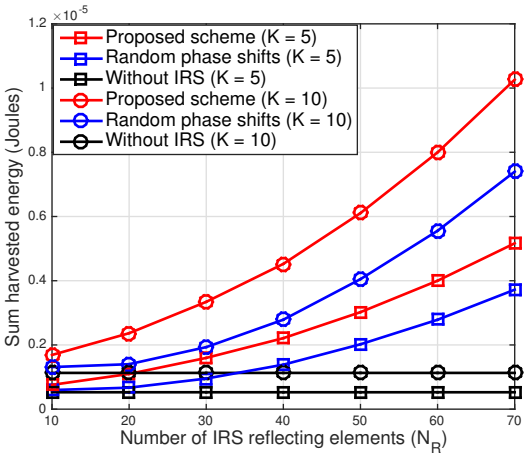

Fig. 11: Sum harvested energy versus number of IRS reflecting element N_R.

respectively. Meanwhile, the IRS brings a further performance gain on sum throughput performance, especially when N_T is large, which verifies the positive impact of the IRS on improving the uplink WIT efficiency. Fig. 8 illustrates the sum throughput performance with respect to different numbers of AP's antennas N_A, and all schemes exhibit a monotonically growing behaviour in terms of N_A. This is due to the fact that increasing N_A enables better utilization of the spatial diversity/multiplexing gain to decode received signals from multiple IoT devices. Larger N_A can better enable the uplink WIT impact of IRS on the sum throughput performance. Similarly, the proposed scheme has a better throughput performance than all the other benchmark schemes, demonstrating the advantage of optimal time scheduling and IRS phase shift designs as well as the employment of IRS.

Moreover, the impact of IRS deployment on the sum throughput is evaluated in Fig. 9, where we consider a scenario that the x-coordinate of IRS, X_{IRS}, varies from -10 to 10. The proposed scheme achieves the nearly same performance as the existing MM-based algorithm, which confirms its effectiveness.. As indicated, all IRS-based schemes first exhibit an slightly increasing behaviour with X_{IRS} and then significantly decline roughly after $X_{IRS} \geq -2$, which significantly outperforms no IRS counterpart (remaining constant with X_{IRS}). This result shows the importance of IRS's position in achieving the maximum sum throughput performance, which also shows that this positive impact of the IRS is maximized in the uplink WIT compared to the scheme without IRS.

In Fig. 10 and Fig. 11, the positive impact of IRS on downlink WET is examined to confirm its importance as well as the optimal design of the IRS beampatterns, and the time scheduling. In Fig. 10, the optimal WET time scheduling τ_0 versus N_R is evaluated with $K = 5$ and $K = 10$. As observed, the proposed scheme exhibits a declining behaviour as N_R increases. It consumes significantly less WET time duration than that without IRS, which is not affected by N_R. This mitigates the total energy consumed at the AP, and allows longer time duration for uplink WIT to enhance the sum throughput. On the other hand, Fig. 11 characterises the sum harvested energy against N_R with $K = 5$ and $K = 10$. Particularly, the sum harvested energy demonstrates a monotonically growing

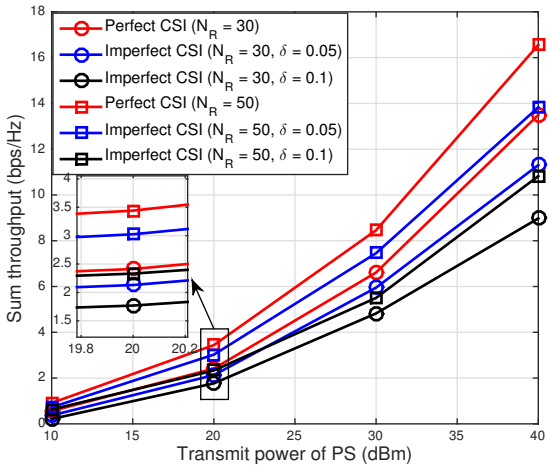

Fig. 12: Sum throughput versus transmit power of PS P_0 for perfect and imperfect CSI scenarios.

trend with N_R, and the proposed scheme can acquire more harvested energy than the other benchmark schemes, which highlights the fact that the improvement of energy harvesting performance is not at the expense of WET time slot as evidenced by Fig. 10. Additionally, the performance advantage of the proposed scheme over other counterparts comes from the optimal design of the WET IRS passive beam pattern, and the improved channel gain at IoT devices by introducing IRS.

Finally, we make a comparison between perfect and imperfect CSI scenarios in terms of sum throughput versus transmit power of PS P_0 in Fig. 12. As expected, the perfect CSI case (i.e., the proposed scheme) exhibits significantly better performance compared to its imperfect counterpart. This is due to the fact that the channel estimation error negatively affects the cascaded CSI, degrading the sum throughput performance. Also, the sum throughput is more sensitive to the larger channel estimation error, which can produce a greater impact on the throughput performance.

V. Conclusion

This paper exploited the sum throughput maximisation problem for IRS-empowered WPCN. This resultant optimisation problem was solved by a two-level procedure, in which the outer level aimed to numerically search for the optimal transmission time scheduling, while the BCD iterative algorithm was proposed to alternately solve the inner-level problem, for optimising receive beamforming, energy beamforming, and IRS phase shifts, respectively. Numerical results were presented to verify convergence of the proposed algorithm and effectiveness of the numerical search method. Moreover, these results highlighted the advantage of optimal IRS phase shift design, optimal time scheduling design, and employment of IRS, compared to existing benchmark schemes.

For future work, we would investigate active-IRS-assisted WPCNs to jointly design the energy beamforming of PS, receive beamforming of AP, IRS active beampattern and time scheduling. For the active IRS, we would not employ the LDT and QT to convert the sum of logarithmically fractional objective functions into the quadratic form. Rather, the numerical solutions, i.e., semi-definite programming and successive convex approximation, could be adopted to solve the IRS active beamforming with the non-convex phase shift constraint. Additionally, we could explore hybrid multiple access (i.e., hybrid TDMA/FDMA scheme) in the IRS-assisted WPCN, to reduce the network overhead. Moreover, the fairness-aware scheme should be considered in the IRS-assisted WPCN, in which the sum rate maximization will be formulated subject to the individual rate constraint to guarantee the QoS of each IoT device.

Appendix

A. *Proof of* Lemma *2*

The convergence of *Algorithm* 2 mainly depends upon the BCD to design the received beamforming, energy beamforming, and the IRS passive beampatterns of downlink WET and uplink WIT in an iterative manner. Now let us prove the convergence of the iterative BCD in *Algorithm* 2. To this end, we fix the time allocation τ_0 to transform problem (7) as follows:

$$\begin{aligned}\max_{\mathbf{w},\mathbf{F},\boldsymbol{\theta},\mathbf{p}} & f\left(\mathbf{w},\mathbf{F},\boldsymbol{\theta},\mathbf{p}\right)=\sum_{k=1}^{K}\log\left(1+\frac{p_k t_{1,k,k}}{\sum_{j\neq k}p_j t_{1,k,j}+\sigma^2\mathbf{f}_k^H\mathbf{f}_k}\right),\\ s.t.\ & (T-\tau_0)p_k\leq\tau_0\eta_k P_0 t_{0,k},\\ & |\theta_{m,n}|=1,\ \forall m\in\{0,1\},\ \forall n\in\{1,...,N_R\},\\ & \|\mathbf{w}\|^2\leq 1.\end{aligned}\tag{49}$$

By applying the LDT, we have

$$\begin{aligned}\max_{\mathbf{w},\mathbf{F},\boldsymbol{\theta},\mathbf{p},\mathbf{r}} & \tilde{f}\left(\mathbf{w},\mathbf{F},\boldsymbol{\theta},\mathbf{p},\mathbf{r}\right)\\ & =\sum_{k=1}^{K}\log\left(1+r_k\right)-\sum_{k=1}^{K}r_k+\sum_{k=1}^{K}\frac{(1+r_k)X_k}{Y_k},\\ s.t.\ & (T-\tau_0)p_k\leq\tau_0\eta_k P_0 t_{0,k},\\ & |\theta_{m,n}|=1,\ \forall m\in\{0,1\},\ \forall n\in\{1,...,N_R\},\\ & \|\mathbf{w}\|^2\leq 1.\end{aligned}\tag{50}$$

Via the QT, we obtain the following problem

$$\begin{aligned}\max_{\mathbf{w},\mathbf{F},\boldsymbol{\theta},\mathbf{p},\mathbf{r},\boldsymbol{\xi}} & \bar{f}\left(\mathbf{w},\mathbf{F},\boldsymbol{\theta},\mathbf{p},\mathbf{r},\boldsymbol{\xi}\right)\\ & =\sum_{k=1}^{K}\log\left(1+r_k\right)-\sum_{k=1}^{K}r_k\\ & +\sum_{k=1}^{K}\Big[2\left[(1+r_k)p_k\right]^{\frac{1}{2}}\Re\left\{\mathrm{conj}\left(\xi_k\right)\tilde{\mathbf{b}}_{k,k}\boldsymbol{\theta}_1+\mathrm{conj}\left(\xi_k\right)\hat{b}_{k,k}\right\}\\ & -|\xi_k|^2\left(\sum_{j=1}^{K}p_j\left|\tilde{\mathbf{b}}_{k,j}\boldsymbol{\theta}_1+\hat{b}_{k,j}\right|^2+\sigma^2\mathbf{f}_k^H\mathbf{f}_k\right)\Big],\\ s.t.\ & (T-\tau_0)p_k\leq\tau_0\eta_k P_0 t_{0,k},\\ & |\theta_{m,n}|=1,\ \forall m\in\{0,1\},\ \forall n\in\{1,...,N_R\},\\ & \|\mathbf{w}\|^2\leq 1.\end{aligned}\tag{51}$$

From the aforementioned three problems, we have,

1) $f\left(\mathbf{w},\mathbf{F},\boldsymbol{\theta},\mathbf{p}\right)\geq\tilde{f}\left(\mathbf{w},\mathbf{F},\boldsymbol{\theta},\mathbf{p},\mathbf{r}\right)$ with equality if and only if $\mathbf{r}$ satisfies $r_k=\frac{X_k}{Y_k}$.

2) $\tilde{f}\left(\mathbf{w},\mathbf{F},\boldsymbol{\theta},\mathbf{p},\mathbf{r}\right) \geq \bar{f}\left(\mathbf{w},\mathbf{F},\boldsymbol{\theta},\mathbf{p},\mathbf{r},\boldsymbol{\xi}\right)$ with equality if and only if $\boldsymbol{\xi}$ satisfies $\xi_k = \frac{[(1+r_k)p_k]^{\frac{1}{2}}\left(\tilde{\mathbf{b}}_{k,k}\boldsymbol{\theta}_1+\hat{b}_{k,k}\right)}{\sum_{j=1}^{K} p_j\left|\tilde{\mathbf{b}}_{k,j}\boldsymbol{\theta}_1+\hat{b}_{k,j}\right|^2+\sigma^2\mathbf{f}_k^H\mathbf{f}_k}$.

Then, we denote l as the iteration index of the BCD in *Algorithm* 7. Also, the variables $\boldsymbol{\xi}^{(l)}$ and $\tilde{\boldsymbol{\xi}}^{(l)}$ are determined by $\xi_k = \frac{[(1+r_k)p_k]^{\frac{1}{2}}\left(\tilde{\mathbf{b}}_{k,k}\boldsymbol{\theta}_1+\hat{b}_{k,k}\right)}{\sum_{j=1}^{K} p_j\left|\tilde{\mathbf{b}}_{k,j}\boldsymbol{\theta}_1+\hat{b}_{k,j}\right|^2+\sigma^2\mathbf{f}_k^H\mathbf{f}_k}$ with $\left(\mathbf{w}^{(l)},\mathbf{F}^{(l)},\boldsymbol{\theta}^{(l)},\mathbf{p}^{(l)},\mathbf{r}^{l}\right)$ and with $\left(\mathbf{w}^{(l+1)},\mathbf{F}^{(l+1)},\boldsymbol{\theta}^{(l+1)},\mathbf{p}^{(l+1)},\mathbf{r}^{l}\right)$, respectively. For the iterative BCD with the ADMM procedures, the following relationships hold

$$
\begin{aligned}
&f\left(\mathbf{w}^{(l+1)},\mathbf{F}^{(l+1)},\boldsymbol{\theta}^{(l+1)},\mathbf{p}^{(l+1)}\right)\\
&\overset{(\alpha_1)}{\geq} \tilde{f}\left(\mathbf{w}^{(l+1)},\mathbf{F}^{(l+1)},\boldsymbol{\theta}^{(l+1)},\mathbf{p}^{(l+1)},\mathbf{r}^{(l+1)}\right)\\
&\overset{(\alpha_2)}{\geq} \tilde{f}\left(\mathbf{w}^{(l+1)},\mathbf{F}^{(l+1)},\boldsymbol{\theta}^{(l+1)},\mathbf{p}^{(l+1)},\mathbf{r}^{(l)}\right)\\
&\overset{(\alpha_3)}{=} \bar{f}\left(\mathbf{w}^{(l+1)},\mathbf{F}^{(l+1)},\boldsymbol{\theta}^{(l+1)},\mathbf{p}^{(l+1)},\mathbf{r}^{(l)},\tilde{\boldsymbol{\xi}}^{(l)}\right)\\
&\overset{(\alpha_4)}{\geq} \bar{f}\left(\mathbf{w}^{(l+1)},\mathbf{F}^{(l+1)},\boldsymbol{\theta}^{(l+1)},\mathbf{p}^{(l+1)},\mathbf{r}^{(l)},\boldsymbol{\xi}^{(l)}\right)\\
&\overset{(\alpha_5)}{\geq} \bar{f}\left(\mathbf{w}^{(l)},\mathbf{F}^{(l)},\boldsymbol{\theta}^{(l)},\mathbf{p}^{(l)},\mathbf{r}^{(l)},\boldsymbol{\xi}^{(l)}\right)\\
&\overset{(\alpha_6)}{=} \tilde{f}\left(\mathbf{w}^{(l)},\mathbf{F}^{(l)},\boldsymbol{\theta}^{(l)},\mathbf{p}^{(l)},\mathbf{r}^{(l)}\right)\\
&\overset{(\alpha_7)}{=} f\left(\mathbf{w}^{(l)},\mathbf{F}^{(l)},\boldsymbol{\theta}^{(l)},\mathbf{p}^{(l)}\right), \qquad (52)
\end{aligned}
$$

where (α_1) follows by *Relation* 1; (α_2) follows the update of $\mathbf{r}$ to maximize $\tilde{f}$ for given other variables; (α_3) follows by *Relation* 2; (α_4) follows the update of $\boldsymbol{\xi}$ to maximizes $\bar{f}$ for given other variables; (α_5) follows the updates of the variables $\mathbf{w}$, $\mathbf{F}$, $\boldsymbol{\theta}$, and $\mathbf{p}$ in Step b) of *Algorithm* 7; (α_6) follows by *Relation* 2; (α_7) follows by *Relation* 1. From aforementioned discussion, the sum throughput objective f produces a monotonically non-decreasing behaviour over iteration. Since the value of f is bounded above, *Algorithm* 2 will converge to a local optimum.

REFERENCES

[1] Z. Chu, F. Zhou, Z. Zhu, R. Q. Hu, and P. Xiao, "Wireless powered sensor networks for internet of things: Maximum throughput and optimal power allocation," *IEEE Internet Things J.*, vol. 5, no. 1, pp. 310–321, Feb. 2018.

[2] R. Zhang and C. K. Ho, "MIMO broadcasting for simultaneous wireless information and power transfer," *IEEE Trans. Wireless Commun.*, vol. 12, no. 5, pp. 1989–2001, May 2013.

[3] S. Bi, C. K. Ho, and R. Zhang, "Wireless powered communication: opportunities and challenges," *IEEE Commun. Mag.*, vol. 53, no. 4, pp. 117–125, 2015.

[4] S. Bi, Y. Zeng, and R. Zhang, "Wireless powered communication networks: an overview," *IEEE Wireless Commun.*, vol. 23, no. 2, pp. 10 – 18, Apr. 2016.

[5] H. Ju and R. Zhang, "Throughput maximization in wireless powered communication networks," *IEEE Trans. Wireless Commun.*, vol. 13, no. 1, pp. 418–428, Jan. 2014.

[6] Renzo, Marco Di, et. al., "Smart radio environments empowered by reconfigurable AI meta-surfaces: an idea whose time has come," *EURASIP J. Wirel. Commun. Netw.*, no. 129, pp. 1–20, May 2019.

[7] M. D. Renzo, A. Zappone, M. Debbah, M. Alouini, C. Yuen, J. D. Rosny, and S. Tretyakov, "Smart radio environments empowered by reconfigurable intelligent surfaces: How it works, state of research, and road ahead," *IEEE J. Sel. Areas Commun.*, vol. 38, no. 11, pp. 2450–2525, Nov. 2020.

[8] Q. Wu and R. Zhang, "Intelligent reflecting surface enhanced wireless network via joint active and passive beamforming," *IEEE Trans. Wireless Commun.*, vol. 18, no. 11, pp. 5394–5409, Nov. 2019.

[9] Q. Wu and R. Zhang, "Towards smart and reconfigurable environment: Intelligent reflecting surface aided wireless network," *IEEE Commun. Mag.*, vol. 58, no. 1, pp. 106–112, Jan. 2020.

[10] H. Guo, Y.-C. Liang, J. Chen, and E. G. Larsson, "Weighted sum-rate maximization for reconfigurable intelligent surface aided wireless networks," *IEEE Trans. Wireless Commun.*, vol. 19, no. 5, pp. 3064 – 3076, May 2020.

[11] Z. Chu, J. Zhong, P. Xiao, D. Mi, W. Hao, J. Shi, and L. Yang, "Unlock self-sustainability of reconfigurable intelligent surface in wireless powered IoT networks," *IEEE Commun. Mag.*, vol. 60, no. 6, pp. 74–80, Jun. 2022.

[12] Z. Chu, Z. Zhu, F. Zhou, M. Zhang, and N. Al-Dhahir, "Intelligent reflecting surface assisted wireless powered sensor networks for internet of things," *IEEE Trans. Commun.*, vol. 69, no. 7, pp. 4877–4889, Jul. 2021.

[13] Z. Chu, Z. Zhu, X. Li, F. Zhou, L. Zhen, and N. Al-Dhahir, "Resource allocation for IRS-assisted wireless-powered FDMA IoT networks," *IEEE Internet Things J.*, vol. 9, no. 11, pp. 8774 – 8785, Jun. 2022.

[14] X. Li, Z. Xie, Z. Chu, V. G. Menon, S. Mumtaz, and J. Zhang, "Exploiting benefits of IRS in wireless powered NOMA networks," *IEEE Trans. Green Commun. Netw.*, vol. 6, no. 1, pp. 175–186, Mar. 2022.

[15] Z. Chu, P. Xiao, D. Mi, W. Hao, M. Khalily, and L.-L. Yang, "A novel transmission policy for intelligent reflecting surface assisted wireless powered sensor networks," *IEEE J. Sel. Topics Signal Process.*, vol. 15, no. 5, pp. 1143–1158, Aug. 2021.

[16] B. Lyu, P. Ramezani, D. T. Hoang, S. Gong, Z. Yang, and A. Jamalipour, "Optimized energy and information relaying in self-sustainable IRS-empowered WPCN," *IEEE Trans. Commun.*, vol. 69, no. 1, pp. 619–633, Jan. 2021.

[17] Q. Wu, X. Zhou, and R. Schober, "IRS-assisted wireless powered NOMA: Do we really need different phase shifts in DL and UL?," *IEEE Wireless Commun. Lett.*, vol. 10, no. 7, pp. 1493–1497, Jul. 2021.

[18] D. Zhang, Q. Wu, M. Cui, G. Zhang, and D. Niyato, "Throughput maximization for IRS-assisted wireless powered hybrid NOMA and TDMA," *IEEE Wireless Commun. Lett.*, vol. 10, no. 9, pp. 1944–1948, Sept. 2021.

[19] M. Hua, Q. Wu, and H. V. Poor, "Power-efficient passive beamforming and resource allocation for IRS-aided WPCNs," *IEEE Trans.Commun.*, vol. 70, no. 5, pp. 3250–3265, May 2022.

[20] Z. Chu, J. Zhong, P. Xiao, D. Mi, W. Hao, R. Tafazolli, and A. Feresidis, "RIS assisted wireless powered IoT networks with phase shift error and transceiver hardware impairment," *IEEE Trans. Commun.*, vol. 70, no. 7, pp. 4910–4924, Jul. 2022.

[21] Z. Chu, P. Xiao, D. Mi, W. Hao, Z. Lin, Q. Chen, and R. Tafazolli, "Wireless powered intelligent radio environment with non-linear energy harvesting," *IEEE Internet Things J.*, vol. 9, no. 18, pp. 18130 – 18141, Sept. 2022.

[22] M. Hua and Q. Wu, "Joint dynamic passive beamforming and resource allocation for IRS-aided full-duplex WPCN," *IEEE Trans. Wireless Commun.*, vol. 21, no. 7, pp. 4829 – 4843, Jul. 2022.

[23] M. Hua and Q. Wu, "Throughput maximization for IRS-aided MIMO FD-WPCN with non-linear EH model," *IEEE J. Sel. Topics Signal Process.*, vol. 16, no. 5, pp. 918–932, Aug. 2022.

[24] Z. Xie, X. Li, M. Zeng, D. Deng, J. Zhang, S. Mumtaz, and A. Nallanathan, "Resource allocation for double IRSs assisted wireless powered NOMA networks," *IEEE Wireless Commun. Lett.*, vol. 12, no. 5, pp. 823–827, May 2023.

[25] K. Cao, H. Ding, L. Lv, Z. Su, J. Tao, F. Gong, and B. Wang, "Physical layer security for intelligent reflecting surface aided wireless powered communication systems," *to appear in IEEE Internet Things J.*, pp. 1–1, 2023.

[26] Z. Zhu, Z. Li, Z. Chu, Q. Wu, J. Liang, Y. Xiao, P. Liu, and I. Lee, "Intelligent reflecting surface-assisted wireless powered heterogeneous networks," *IEEE Trans. Wireless Commun.*, pp. 1–1, 2023.

[27] B. L. J. Liao, W. Wu, and Y. Li, "Intelligent reflecting surface assisted secure computation of wireless powered MEC system," *to appear in IEEE Trans. Mobile Comput.*, pp. 1–12, 2023.

[28] L. Zhai, Y. Zou, J. Zhu, and Y. Jiang, "Stackelberg game-based multiple access design for intelligent reflecting surface assisted wireless powered IoT networks," *IEEE Trans. Wireless Commun.*, pp. 1–1, 2023.

[29] Y. Xu, Z. Gao, Z. Wang, C. Huang, Z. Yang, and C. Yuen, "RIS-enhanced WPCNs: Joint radio resource allocation and passive beam-

forming optimization," *IEEE Trans. Vehicular Technol.*, vol. 70, no. 8, pp. 7980–7991, Aug. 2021.

[30] C. Wu, F. Ke, X. Yang, M. Wen, D. Li, and X. Zhang, "Joint energy and information precoding for NOMA-based WPCNs aided by reconfigurable intelligent surface," *IEEE Trans. Vehicular Technol.*, pp. 1–13, 2023.

[31] Z. Wang, L. Liu, and S. Cui, "Channel estimation for intelligent reflecting surface assisted multiuser communications: Framework, algorithms, and analysis," *IEEE Trans. Wireless Commun.*, vol. 19, no. 10, pp. 6607–6620, Oct. 2020.

[32] G. Zhou, C. Pan, H. Ren, K. Wang, and A. Nallanathan, "A framework of robust transmission design for IRS-aided MISO communications with imperfect cascaded channels," *IEEE Trans. Signal Process.*, vol. 68, pp. 5092–5106, Aug. 2020.

[33] Y. Omid, S. M. Shahabi, C. Pan, Y. Deng, and A. Nallanathan, "Low-complexity robust beamforming design for IRS-aided MISO systems with imperfect channels," *IEEE Communications Letters*, vol. 25, no. 5, pp. 1697–1701, May 2021.

[34] S. Hong, C. Pan, H. Ren, K. Wang, K. K. Chai, and A. Nallanathan, "Robust transmission design for intelligent reflecting surface-aided secure communication systems with imperfect cascaded CSI," *IEEE Trans. Wireless Commun.*, vol. 20, no. 4, pp. 2487–2501, Apr. 2021.

[35] K. Shen and W. Yu, "Fractional programming for communication systems - part ii: Uplink scheduling via matching," *IEEE Trans. Signal Process.*, vol. 66, no. 10, pp. 2631 – 2644, May 2018.

[36] H. Niu, Z. Chu, F. Zhou, Z. Zhu, M. Zhang, and K.-K. Wong, "Weighted sum secrecy rate maximization using intelligent reflecting surface," *IEEE Trans. Comm.*, vol. 69, no. 9, pp. 6170–6184, Sept. 2021.